

## Accepted Manuscript

Synthesis, characterization, anti-diabetic potential and DFT studies of 7-hydroxy-4-methyl-2-oxo-2H-chromene-8-carbaldehyde oxime

Seyed Mohammad Bagher Hosseini Ghazvini, Parvin Safari, Akbar Mobinikhaledi, Hassan Moghanian, Hassan Rasouli



PII: S1386-1425(18)30662-0  
DOI: doi:[10.1016/j.saa.2018.07.009](https://doi.org/10.1016/j.saa.2018.07.009)  
Reference: SAA 16278

To appear in: *Spectrochimica Acta Part A: Molecular and Biomolecular Spectroscopy*

Received date: 24 November 2017

Revised date: 30 June 2018

Accepted date: 5 July 2018

Please cite this article as: Seyed Mohammad Bagher Hosseini Ghazvini, Parvin Safari, Akbar Mobinikhaledi, Hassan Moghanian, Hassan Rasouli, Synthesis, characterization, anti-diabetic potential and DFT studies of 7-hydroxy-4-methyl-2-oxo-2H-chromene-8-carbaldehyde oxime. Saa (2018), doi:[10.1016/j.saa.2018.07.009](https://doi.org/10.1016/j.saa.2018.07.009)

This is a PDF file of an unedited manuscript that has been accepted for publication. As a service to our customers we are providing this early version of the manuscript. The manuscript will undergo copyediting, typesetting, and review of the resulting proof before it is published in its final form. Please note that during the production process errors may be discovered which could affect the content, and all legal disclaimers that apply to the journal pertain.

## Synthesis, characterization, anti-diabetic potential and DFT studies of 7-hydroxy-4-methyl-2-oxo-2*H*-chromene-8-carbaldehyde oxime

Seyed Mohammad Bagher Hosseini Ghazvini<sup>a,\*†</sup>, Parvin Safari<sup>at</sup>, Akbar Mobinikhaledi<sup>a</sup>, Hassan Moghanian<sup>b</sup>, Hassan Rasouli<sup>c</sup>

<sup>a</sup> Department of Chemistry, Faculty of Science, Arak University, Arak, Iran

<sup>b</sup> Department of Chemistry, Dezful Branch, Islamic Azad University, Dezful, Iran

<sup>c</sup> Medical Biology Research Center, Kermanshah University of Medical Sciences, Kermanshah, Iran

\* Correspondence: Smbhgh@yahoo.com

### Abstract

A new compound named 7-hydroxy-4-methyl-2-oxo-2*H*-chromene-8-carbaldehyde oxime (7-Oxime) was synthesized and characterized by FT-IR, FT-Raman, <sup>1</sup>H-NMR and <sup>13</sup>C-NMR techniques. The conformer possibilities were studied to find the most stable conformer and its molecular geometry. Then, the dimer form of the most stable monomer was built and optimized. Density functional theory (DFT) B3LYP method with 6-311++G(d,p) basis set was applied to analyze the molecular electrostatic potential (MEP), HOMO and LUMO orbitals, the vibrational wavenumbers, the infrared intensities, the Raman scattering activities and several thermodynamic properties (at different temperatures). The stability of the molecule derived from hyperconjugative interactions and charge delocalization has been analyzed by using natural bond orbital (NBO) analysis. In order to find the possible inhibitory activity of 7-Oxime, an accurate molecular blind docking was performed. The results indicated that the mentioned compound has a good binding affinity to interact with the active sites of human  $\alpha$ -glucosidase and  $\alpha$ -amylase. For the first time, our computational finding suggests that this compound can have potential to be used as a supplementary agent in the pre-management of diabetes mellitus.

### Keywords

7-Oxime; Vibrational spectra; NMR spectra; FMO; Molecular docking; diabetes mellitus

## 1. Introduction

Nowadays, the biological and pharmacological properties of coumarin and its derivatives have received many attentions from pharmaceutical and food industries [1]. These natural secondary metabolites exhibit a wide range of biological activities including anticancer and anti-diabetic effects [2-4]. These compounds are widely used as fragrance, pharmaceuticals, agrochemicals, laser dyes, optical brighteners and fluorescent markers [5, 6]. Among coumarins, hydroxycoumarins are one of the most important classes of plant-derived secondary metabolites with significant antioxidant activities and extensive applications [7]. These compounds have originated from many different classes of plant sources. As can be seen in Fig. 1, the structure of these compounds includes molten benzene and  $\alpha$ -pyrone rings [7] (Fig. 1).

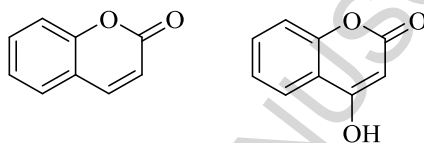


**Fig. 1.** The chemical structures of coumarin (Left) and 4-hydroxycoumarin (Right)

Many studies have indicated that computer-based drug design strategies have a central role in the development of new drugs [8, 9]. Among computational techniques, Density functional theory (DFT) is a promising method for the evaluation of vibrational modes, bonding and structural properties of organic molecules [10-12]. Besides, these computational approaches have been used to investigate the vibrational spectra and the other electronic features of coumarins and its derivatives [13].

Therefore, the aim of the current study was to investigate the structural, electronic and spectroscopic properties of a new compound named 7-hydroxy-4-methyl-2-oxo-2*H*-chromene-8-carbaldehyde oxime (7-Oxime) through experimental (FT Raman, FT-IR and NMR) and computational DFT-based methods. Indeed, the anti-diabetic potential of this compound was investigated via molecular docking simulation.

## 2. Methods

### 2.1. Experimental Section

#### 2.1.1. Synthesis of 7-Oxime

As can be seen in Fig. 2, 7-Oxime was synthesized according to the following steps.

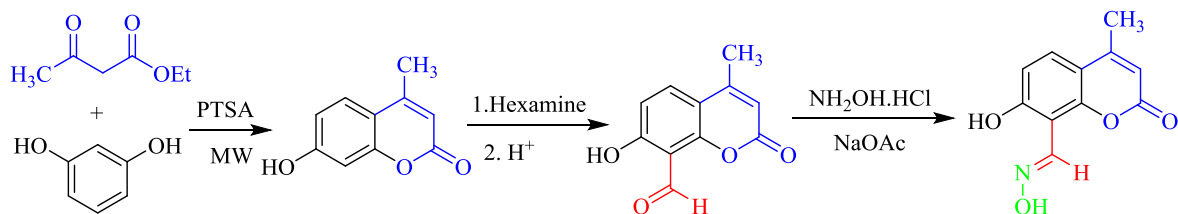


Fig. 2. Synthesis of 7-Oxime.

#### A. Synthesis of 8-formyl-7-hydroxy-4-methylcoumarin

The method reported previously (with some slight modifications) [14, 15] was used for the synthesis of 8-Formyl-7-hydroxy-4-methylcoumarin. First, *p*-Toluenesulfonic acid (*p*-TSA, 0.36 g, 2.0 mmol) was added to a mixture of resorcinol (4.4 g, 40 mmol) and ethyl acetoacetate (5.2 g, 40 mmol) and the mixture was irradiated using the microwave oven for 30 s at 450 W power. Then, the mixture was cooled to room temperature and a mixture of ethanol: water (1:1) was added to it. The mixture was stirred for 5 min and the solid was separated by filtering and dried to give 7-hydroxy-4-methylcoumarin (yield 95%; mp: 184–186 °C).

In the second step, 7-hydroxy-4-methylcoumarin (5 g, 28.4 mmol) and hexamine (5.6 g, 40 mmol) were added to glacial acetic acid (90 ml) and the mixture was heated for 4 h. Next, hexamine (5.6 g, 40 mmol) was added to the mixture and heated for another 4 h. After the reaction was completed (monitored by TLC), hydrochloric acid (20%, 70 ml) was added and the mixture was heated for 40 min. Then, the mixture was cooled and extracted with ether (50 ml) twice. The combined organic layer was concentrated under the reduced pressure to give the crude product. Then, the crude product was re-crystallized from ethanol to obtain pure 8-formyl-7-hydroxy-4-methylcoumarin (yield 18%; mp: 145–146 °C).

#### B. Synthesis of 7-hydroxy-4-methyl-2-oxo-2H-chromene-8-carbaldehyde oxime

7-hydroxy-4-methylcoumarin (2 mmol), hydroxylamine hydrochloride (6 mmol) and sodium acetate (6 mmol) were dissolved in ethanol (95%, 10 ml) and the solution was refluxed for 6 h. Then, the solution was cooled down to room temperature. The white product was filtered off and washed with cold ethanol (yield 89%; mp: 190-192 °C). The spectral data of this compound has been represented below.

FT-IR (in KBr pellet)  $\nu_{\max}$  ( $\text{cm}^{-1}$ ): 3297 (OH of oxime group), 3084, 1692 (C=O of lactone), 1616 (C=N of oxime group), 1393, 1366, 1080 (C-O-C of pyrone), 993;  $^1\text{H}$  NMR (400 MHz, DMSO- $d_6$ ):  $\delta$  = 11.946 (s, 1H, OH of oxime group), 11.164 (s, 1H, OH, phenolic), 8.531 (s, 1H, CH of oxime group), 7.660 (d,  $J$  = 8.8 Hz, 1H, CH of ring 2), 6.934 (d,  $J$  = 8.8 Hz, 1H, CH of ring 2), 6.227 (s, 1H, CH, vinyl of ring 1), 2.510 (s, 3H,  $\text{CH}_3$ );  $^{13}\text{C}$  NMR (100 MHz, DMSO- $d_6$ ):  $\delta$  = 159.703 (C-OH of ring 2), 159.208 (C-H of oxime group), 153.657 (C=O of lactone), 151.772, 144.023, 127.227, 112.810, 112.065, 110.728, 104.942, 18.271 ( $\text{CH}_3$ )

### 2.1.2. The measurement of FT-IR and FT-Raman spectra

A Unicom Galaxy Series FT-IR 5000 spectrophotometer was used to record the FT-IR spectra of the samples in the range of 400-4000  $\text{cm}^{-1}$ . The spectra were recorded with a resolution of 1  $\text{cm}^{-1}$  and the signals were the results of 15 scans (averagely). A Bruker RFS 100/S FT-Raman was used for recording FT-Raman spectrum of the sample by using 1064 nm line of Nd:YAG laser as excitation wavelength in the region of 800-4000  $\text{cm}^{-1}$ . The detector was a liquid nitrogen cooled Ge detector. Five hundred scans were collected at 4  $\text{cm}^{-1}$  resolution by using a laser power of 100 mW.

### 2.1.3. The measurement of NMR spectra

The  $^1\text{H}$  and  $^{13}\text{C}$  NMR spectra were collected in DMSO- $d_6$  with TMS as an internal standard on a Bruker Avance spectrometer operating at 400 and 100 MHz for proton-1 and carbon-13 atoms, respectively.

## 2.2. Computational methods

The computational calculations were performed at DFT level with the Becke's three-parameter hybrid functional (B3) [16] for the exchange part and the Lee-Yang-Parr (LYP) correlation function [17]. Gaussian 03 suite of quantum chemical codes [18] was used for this purpose without any constraint in the geometry with split-valence triple-zeta basis set along with diffuse and polarization function (6-311++G(d,p)).

First, the structure of 7-Oxime was constructed using GaussView program [19]. Next, the sixteen possible conformations of the mentioned compound, their corresponding energies and harmonic vibrational frequencies were calculated by B3LYP method with 6-311++G(d,p) basis set in DMSO

and the vacuum. The most stable conformer was detected based on  $\Delta E = E_{\text{Mean}} - E_{\text{N}}$  formula. As shown in Fig. 4, the dimer form was made of two units of the most stable conformer of the monomer (A2). The absence of imaginary frequency verified that the optimized geometry of the dimer and monomer form was true minima on the potential energy surface at B3LYP method with 6-311++G(d,p) level of theory by assuming  $C_2$  and  $C_s$  point group symmetry for the dimer and monomer form, respectively. Computational analysis was performed to calculate the optimized geometrical parameters, energy, fundamental vibrational frequencies, IR intensity, Raman activity, FMOs analysis, NBO analysis, NMR analysis, dipole moments and other thermodynamical parameters.

It is essential to scale down the calculated harmonic frequencies to improve the agreement between the calculated and the experimental values. Hence, the calculated vibrational frequencies above  $1700 \text{ cm}^{-1}$  were scaled by 0.958 while those calculated below  $1700 \text{ cm}^{-1}$  were scaled by 0.983 by B3LYP method [20]. Furthermore, the theoretical vibrational spectra of the title compound were interpreted by means of potential energy distribution (PED) via VEDA program [21]. GaussView program [19] was also utilized to get visual animation and to verify the normal modes assignment. In addition, the Raman activities ( $S_i$ ) calculated by Gaussian 03 program [18] was converted to relative Raman intensities ( $I_i$ ) by using Eq. 1. This formula has been derived from the intensity theory of Raman scattering [22, 23]:

$$I_i = \frac{f(\nu_0 - \nu_i)^4 S_i}{\nu_i [1 - \exp(-(hc\nu_i)/(kT))]} , \text{ Eq. (1)}$$

Where  $\nu_0$  was the laser exciting wavenumber in  $\text{cm}^{-1}$ ,  $\nu_i$  was the vibrational wavenumber of the normal mode and  $h$ ,  $c$ ,  $k$  and  $f$  universal constants were suitably chosen as common normalization factor for the intensity of all peaks.

The NBO analyses were performed via NBO 5.0 tool [24] implemented in the Gaussian 03 [18] program at B3LYP/6-311++G(d,p) level. The molecular electrostatic potential (MEP) was measured to study the reactive sites of the monomer form, to explain the possible reactivity sites for building the dimer form and to correct chemical model in NMR analysis. Afterward, the  $^{13}\text{C}$  and  $^1\text{H}$  NMR isotropic shifts were calculated by GIAO method [11, 25] using the optimized geometry of the dimer and monomer form in both DMSO and the vacuum.

### 2.2.1. Molecular docking

Today, molecular docking plays a central role in drug discovery [26-28]. This method can show an accurate view about ligand-protein interactions [29, 30]. In fact, this method has been considered as one of the an interesting methods for structural studies despite the fact that it is a primitive approach for finding the interaction between proteins and ligands [31, 32]. So, molecular docking simulation (fully blind docking) was performed to investigate the possible inhibitory property of 7-Oxime against enzyme involved in type 2 diabetes mellitus. The 3D crystallographic structure of human lysosomal  $\alpha$ -glucosidase (PDB ID: 5NN8 [33]) and human  $\alpha$ -amylase (PDB ID: 1HNY[34]) were downloaded from the Protein Databank RCSB PDB and then used as favorable receptors to perform molecular docking. AutoDock 4.2.6 [35] software was used for molecular docking, and LigPlot<sup>+</sup> [6] and PyMOL (<https://pymol.org/>) tools were used to visualize the results. The DruLio tool [36, 37] was used for Drug-likeness and ADMET prediction.

## 3. Results and discussion

### 3.1. Conformational stability

The possible conformers of 7-Oxime were derived from the orientation of the hydroxyl and oxime groups in the eighth and the ninth position, respectively. Fig. 3 shows the possible sixteen conformers for the mentioned compound. In order to find the most energetically stable configuration of 7-Oxime, all of the possible conformers were optimized at B3LYP/6-311++G(d,p) level in the vacuum and DMSO.

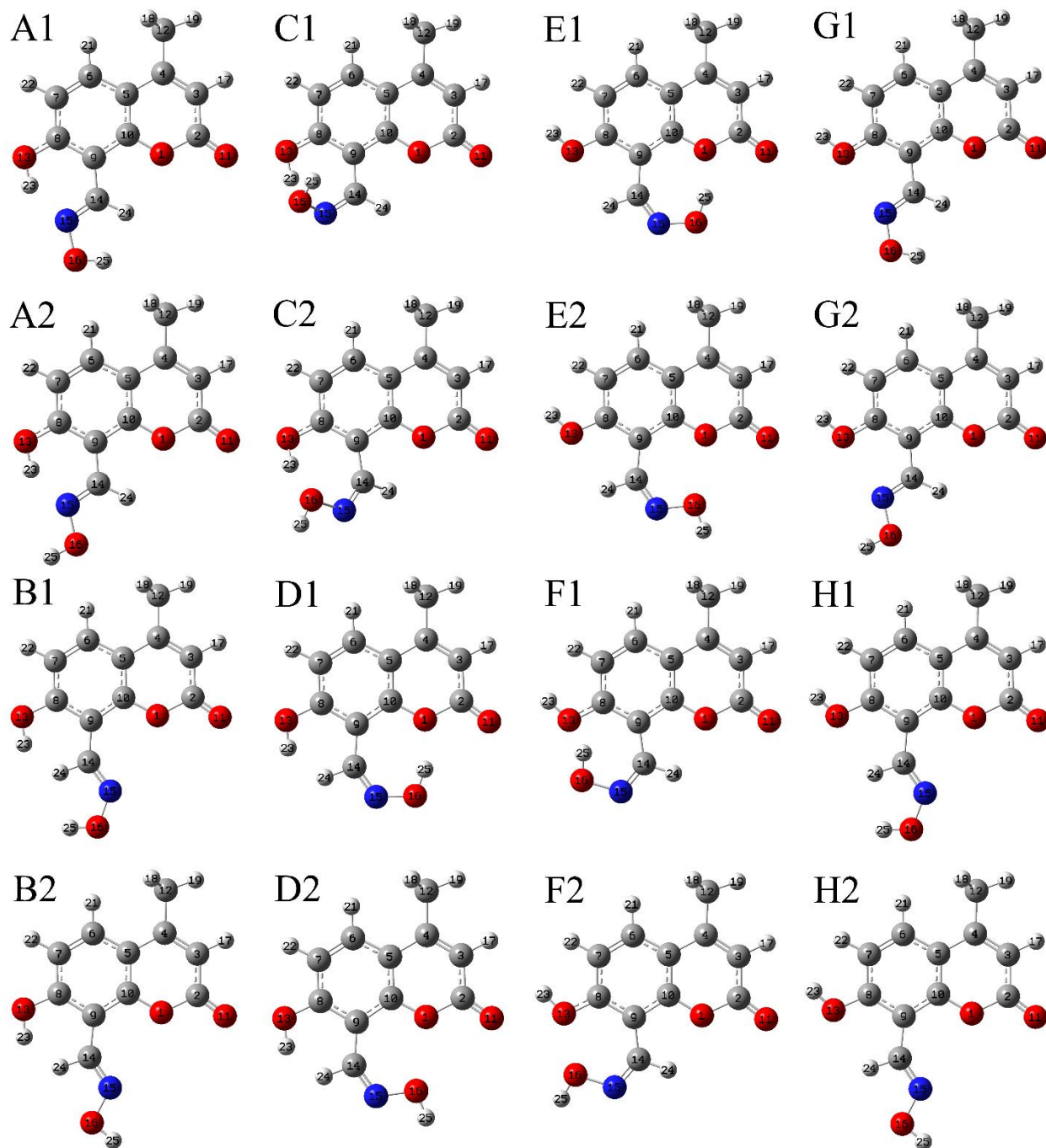


**Fig. 3.** Different conformer possibilities of 7-Oxime

The results indicated that the oxime group adopted "E" configuration in A1, A2 and B1, B2 conformers when the dihedral angle of C<sub>9</sub>-C<sub>8</sub>-O<sub>13</sub>-H<sub>23</sub> was equal with 0°. The only difference between the conformers A1 and A2 as well as B1 and B2 was the dihedral angle of C<sub>14</sub>=N<sub>15</sub>-O<sub>16</sub>-H<sub>25</sub> in the oxime group. The dihedral angle of C<sub>14</sub>=N<sub>15</sub>-O<sub>16</sub>-H<sub>25</sub> was adopted 0° for A1, B1 and 180° for A2, B2 conformers. In addition, the dihedral angle of C<sub>9</sub>-C<sub>8</sub>-O<sub>13</sub>-H<sub>23</sub> was 0° and the

configuration was "Z" for C1, C2 and D1, D2 conformers. The dihedral angle of the oxime group in C1, D1 and C2, D2 conformers was 0° and 180°, respectively. Also, the dihedral angle of C<sub>9</sub>-C<sub>8</sub>-O<sub>13</sub>-H<sub>23</sub> was 180° in E1, E2, F1, F2, G1, G2, H1 and H2. However, the configuration of the oxime group in E1, E2, F1, F2 conformers was "Z" while G1, G2, H1, H2 conformers had "E" configuration. Besides, the dihedral angles of the oxime group for E1, F1, G1, H1 and E2, F2, G2, H2 conformers were obtained to be 0° and 180°, respectively.

All sixteen possible conformers were optimized in the vacuum and DMSO. As detailed in **Table 1**, B1, B2, D1, D2, E1, E2, H2 conformers (in both DMSO and the vacuum) and H1 (in the vacuum) have imaginary wavenumbers. According to our results, the conformer was more stable when the configuration of the oxime group was E and the dihedral angle of C<sub>9</sub>-C<sub>8</sub>-O<sub>13</sub>-H<sub>23</sub> was equal with 0°. The order of conformer stability was A2> A1> C1> C2 and A2> A1> G2> C2 in the vacuum and DMSO, respectively. In both DMSO and the vacuum, the favored conformer A2 with dihedral angle of C<sub>14</sub>=N<sub>15</sub>-O<sub>16</sub>-H<sub>25</sub> (180°) in the oxime group. The energy differences between the most stable (A2) and the second stable (A1) conformer were -4.177 and -3.171 kcal mol<sup>-1</sup> in the vacuum and DMSO, respectively. The mean deviation of energy differences between the conformer possibilities has been shown in Fig. S.1.

**Table 1.** Calculated total energies ( $E^{tot}$ ) and relative  $\Delta E^a$  (kcal/mol) energies of the conformer possibilities studied by B3LYP methods with 6-311++G(d,p) basis set

Conformer possibilities <sup>b</sup>		Gas			DMSO		
		$E^{tot}$	$\Delta E^a$	Nimag <sup>c</sup>	$E^{tot}$	$\Delta E^a$	Nimag <sup>c</sup>
1	A1	-489718.900	9.668	0	-489736.249	5.318	0
2	A2	-489723.017	13.785	0	-489739.420	8.489	0
3	B1	-489701.486	-7.746	1: [-210.21 cm <sup>-1</sup> ]	-489727.108	-3.823	2: [-174.68, -21.32 cm <sup>-1</sup> ]
4	B2	-489709.452	0.220	1: [-152.57 cm <sup>-1</sup> ]	-489730.873	-0.058	2: [-157.02, -24.09 cm <sup>-1</sup> ]
5	C1	-489717.636	8.404	0	-489734.972	4.041	0
6	C2	-489717.636	8.404	0	-489734.972	4.042	0
7	D1	-489702.453	-6.778	1: [-184.23 cm <sup>-1</sup> ]	-489720.864	-10.067	2: [-159.98, -50.21 cm <sup>-1</sup> ]
8	D2	-489700.756	-8.476	1: [-203.03 cm <sup>-1</sup> ]	-489721.732	-9.199	1: [-138.78 cm <sup>-1</sup> ]
9	E1	-489703.628	-5.604	1: [-77.32 cm <sup>-1</sup> ]	-489725.321	-5.610	1: [-72.56 cm <sup>-1</sup> ]
10	E2	-489702.801	-6.431	1: [-106.37 cm <sup>-1</sup> ]	-489726.160	-4.770	1: [-98.73 cm <sup>-1</sup> ]
11	F1	-489705.693	-3.539	0	-489729.343	-1.588	0
12	F2	-489709.947	0.715	0	-489733.943	3.012	0
13	G1	-489706.898	-2.334	0	-489732.107	1.176	0
14	G2	-489711.761	2.530	0	-489735.414	4.483	0
15	H1	-489704.639	-4.593	1: [-33.22 cm <sup>-1</sup> ]	-489731.443	0.512	0
16	H2	-489711.008	1.776	1: [-25.40 cm <sup>-1</sup> ]	-489734.973	4.042	1: [-31.98 cm <sup>-1</sup> ]

<sup>a</sup>  $\Delta E = E_{\text{Mean}} - E_{\text{N}}$

<sup>b</sup> See conformer possibilities for the title compound in **Fig. 3**.

<sup>c</sup> The number of imaginary wavenumbers (cm<sup>-1</sup>).

In the most stable conformer (*i.e.* A2), the hydroxyl group was planar with the ring and the oxime moiety probably due to the strong conjugation, resonance, and hydrogen-bonding interactions.

### 3.2. Molecular geometry

Fig. 4 illustrates the optimized molecular structure of 7-Oxime with the  $C_s$  point group symmetry of the monomer and  $C_2$  point group symmetry of the dimer form. In this molecule, the coumarin ring was substituted with the following groups: methyl at  $C_4$ , hydroxyl at  $C_8$  and oxime at  $C_9$ . The optimized values of the bond lengths and bond angles have been detailed in Table 2. To confirm the chemical structure of 7-Oxime, it was compared with the crystalline structure of its analogous compound (8-[(Hydrazinylidene)methyl]-4-methyl-2-oxo-2*H*-chromen-7-yl 4-methylbenzenesulfonate) [38]. The results showed that the bond lengths and bond angles of 7-Oxime (*i.e.* the most stable conformer) were larger than the observed queries in the experimental assays. It can be explained by the fact that the calculations belonged to the isolated molecule in the vacuum while the experimental results belonged to the molecule in solid state and the values of the bond lengths and bond angles depended on the interaction between molecules in the crystal lattice [13].

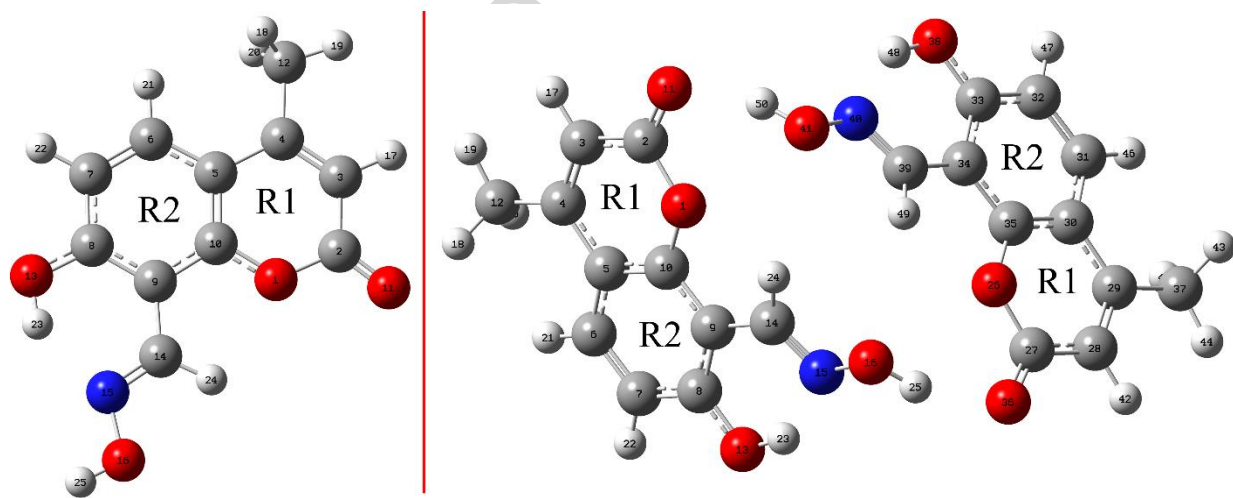


**Fig. 4.** Molecular structure of 7-Oxime along with numbering of atoms (both monomer and dimer forms)

7-Oxime was a cyclic and aromatic compound due to the continuous delocalization of electrons in the coumarin ring. The dihedral angles of  $C_4-C_5-C_{10}-C_9 = 180^\circ$  and  $C_6-C_5-C_{10}-O_1 = 180^\circ$  confirmed that 7-Oxime was planar (Table 2). It has eleven C-C, seven C-H, four C-O, one C-N, one N-O

and two O-H bonds and the length of C-C bonds in the coumarin ring was not the same due to the electron donating of hydroxyl group, electron withdrawing of the oxime group and the inductive–mesmeric interactions with the methyl group which consequently led to the contraction of some C-C bonds and the expansion of the others.

The experimental values of these C-C bond lengths fell in the range of 1.342–1.497 Å while those obtained by computational method fell in the range of 1.3575–1.5036 Å. The DFT calculations showed that the bond length of C<sub>3</sub>-C<sub>4</sub> was shortened and it was 1.3575 Å, proving the presence of double bond character. Also, C<sub>9</sub>-C<sub>14</sub> bond length was obtained to be 1.461 Å and 1.4563 Å by experimental and DFT methods, respectively. This bond was the largest C-C bond in the coumarin ring of our compound.

In addition, the interaction between the hydroxyl and the oxime groups in 7-Oxime compound can affect the regular hexagonal structure. The calculated bond angles represented in Table 2 were good evidence for this effect. For example, C<sub>7</sub>-C<sub>6</sub>-C<sub>5</sub> and C<sub>10</sub>-C<sub>5</sub>-C<sub>6</sub> angles were obtained to be 121.635 Å and 117.524 Å, respectively. In addition, a significant deviation from trigonality was observed in the bond angle of C<sub>3</sub>-C<sub>2</sub>-O<sub>11</sub> (127.364 Å according to B3LYP and 126.59 Å according to the experimental results) due to the electronic repulsion between O<sub>11</sub> and O<sub>1</sub> atoms.

Also, the corresponding dihedral angles N<sub>15</sub>-C<sub>14</sub>-C<sub>9</sub>-C<sub>8</sub> = 0° and H<sub>23</sub>-O<sub>13</sub>-C<sub>8</sub>-C<sub>9</sub> = 0° confirmed that the hydrogen atom of the hydroxyl group and the nitrogen atom of the oxime group were exactly in the same plane with the aromatic ring.

There is an intramolecular hydrogen bond between the proton of the hydroxyl group and the nitrogen of the oxime group. The length of this hydrogen bond (H<sub>23</sub>...N<sub>15</sub>) was equal with 1.76985 Å.

To confirm the computational results, the linear regression analysis was applied between the theoretical (at B3LYP/6-311++G(d,p) level in the vacuum) and experimental bond lengths as well as theoretical (at B3LYP/6-311++G(d,p) level in the vacuum) and experimental bond angles. The linear correlation coefficients (R<sup>2</sup>) values, obtained by B3LYP/6-311++G(d,p) level, were 0.9741 (for the bond lengths) and 0.8805 (for the bond angles), respectively.

To investigate the influence of the intermolecular interactions, the geometry was also optimized for the dimer form of 7-Oxime. The distances between O<sub>16</sub>-H<sub>25</sub>...O<sub>36</sub> and O<sub>41</sub>-H<sub>50</sub>...O<sub>11</sub> were 1.878 and 1.878 Å, respectively. These relatively short distances were probably due to the strong intermolecular interactions. Also, the distances between O<sub>16</sub>...O<sub>36</sub> and O<sub>11</sub>...O<sub>41</sub> were 2.821 and

2.821 Å, respectively. As a result, the investigation showed that  $R^2$  value of the dimer form was better than that of the monomer form.

**Table 2.** The optimized parameters calculated for 7-Oxime

Bond lengths (Å)	Bond lengths (Å)			Bond angles (°)	Bond angles (°)		
	Monomer	Dimer	Experimental <sup>a</sup>		Monomer	Dimer	Experimental <sup>a</sup>
R(1,2)	1.406	1.383	1.378 (18)	A(2,1,10)	122.940	123.152	121.770 (12)
R(1,10)	1.358	1.362	1.374 (18)	A(1,2,3)	115.540	116.318	117.100 (14)
R(2,3)	1.447	1.440	1.442 (2)	A(1,2,11)	117.090	116.614	116.300 (15)
R(2,11)	1.202	1.217	1.203 (2)	A(3,2,11)	127.360	127.067	126.590 (15)
R(3,4)	1.357	1.362	1.342 (2)	A(2,3,4)	122.960	122.252	122.850 (14)
R(3,17)	1.082	1.082	0.930	A(2,3,17)	115.180	115.780	118.600
R(4,5)	1.450	1.446	1.453 (2)	A(4,3,17)	121.870	121.952	118.600
R(4,12)	1.504	1.503	1.497 (2)	A(3,4,5)	119.130	119.279	118.530 (14)
R(5,6)	1.410	1.412	1.395 (2)	A(3,4,12)	120.750	120.555	121.580 (15)
R(5,10)	1.403	1.403	1.394 (2)	A(5,4,12)	120.120	120.164	119.840 (15)
R(6,7)	1.378	1.378	1.376 (2)	A(4,5,6)	124.300	124.868	123.600 (14)
R(6,21)	1.083	1.083	0.930	A(4,5,10)	118.180	118.011	118.630 (14)
R(7,8)	1.404	1.407	1.382 (2)	A(6,5,10)	117.520	117.117	117.710 (14)
R(7,22)	1.082	1.083	0.930	A(5,6,7)	121.630	121.359	120.700 (15)
R(8,9)	1.414	1.413	1.397 (2)	A(5,6,21)	119.350	119.516	119.700
R(8,13)	1.340	1.337	1.412 (18)	A(7,6,21)	119.030	119.121	119.700
R(9,10)	1.410	1.405	1.409 (2)	A(6,7,8)	120.200	120.518	119.700 (15)
R(9,14)	1.456	1.459	1.461 (2)	A(6,7,22)	121.550	121.398	120.200
R(12,18)	1.094	1.094	0.960	A(8,7,22)	118.240	118.079	120.200
R(12,19)	1.090	1.090	0.960	A(7,8,9)	120.390	120.244	123.110 (14)
R(12,20)	1.094	1.094	0.960	A(7,8,13)	117.570	117.913	117.970 (13)
R(13,23)	0.985	0.990	-	A(9,8,13)	122.040	121.843	118.910 (13)
R(14,15)	1.283	1.283	1.273 (19)	A(8,9,10)	117.770	117.384	114.760 (13)
R(14,24)	1.087	1.088	0.930	A(8,9,14)	122.520	122.588	125.940 (13)
R(15,16)	1.396	1.381	-	A(10,9,14)	119.710	120.027	119.300 (13)
R(16,25)	0.964	0.981	-	A(1,10,5)	121.250	120.827	120.980 (13)
				A(1,10,9)	116.260	115.856	115.200 (13)
Dihedral angle (Å)				A(5,10,9)	122.480	123.311	123.800 (14)
		Monomer	Dimer	A(4,12,18)	111.020	110.908	109.500
C <sub>6</sub> -C <sub>5</sub> -C <sub>10</sub> -O <sub>1</sub>		180.000	178.659	A(4,12,19)	110.880	110.949	109.500
C <sub>9</sub> -C <sub>10</sub> -C <sub>5</sub> -C <sub>4</sub>		180.000	179.692	A(4,12,20)	111.020	110.961	109.500
N <sub>15</sub> -C <sub>14</sub> -C <sub>9</sub> -C <sub>8</sub>		0.000	11.827	A(18,12,19)	108.260	108.346	109.500
H <sub>23</sub> -O <sub>13</sub> -C <sub>8</sub> -C <sub>9</sub>		0.000	2.858	A(18,12,20)	107.260	107.260	109.500
				A(19,12,20)	108.260	108.282	109.500
Intramolecular H bond lengths and angles:				A(8,13,23)	108.940	108.726	-
		Monomer	Dimer	A(9,14,15)	120.510	120.108	122.140 (14)
R(15,23)		1.770	1.771	A(9,14,24)	118.980	119.241	118.900
A(13,23,15)		144.400	144.685	A(15,14,24)	120.510	120.650	118.900
A(23,15,14)		101.580	100.983	A(14,15,16)	112.290	112.742	-
				A(15,16,25)	103.850	105.258	-
Comparison of bond lengths:				Comparison of bond angles:			
Monomer		Dimer		Monomer		Dimer	
$R_{\text{exp}} = 1.3934$		$R_{\text{exp}} = 1.4081$		$A_{\text{exp}} = 0.936$		$A_{\text{exp}} = 0.9411$	
$R_{\text{B3LYP}} = 0.5559$		$R_{\text{B3LYP}} = 0.5742$		$A_{\text{B3LYP}} + 7.5593$		$A_{\text{B3LYP}} + 6.9390$	
$R^2 = 0.9741$ , RMSD = 0.0821		$R^2 = 0.9773$ , RMSD = 0.0822		$R^2 = 0.8805$ , RMSD = 1.6251		$R^2 = 0.8879$ , RMSD = 1.5715	

<sup>a</sup> Taken from Ref [38].

### 3.3. Vibrational frequencies

7-Oxime consisted of 25 atoms so it has 69 normal vibrational modes. Also, the molecule structure of the title compound has  $C_s$  point group symmetry.

It should be noted that the calculations were performed for a free molecule in the vacuum while the experiments were done in the solid phase. Thus, the observed differences between the

calculated frequencies and the experimental assay could be due to a crystal field effect arising from the intermolecular interactions [13]. So, the calculated harmonic frequencies were scaled by introducing scaling factors to improve the agreement between the calculated and the experimental results [20].

The experimental assignments of the FT-IR and FT-Raman spectra for several vibrations, unscaled and scaled vibrational frequencies, Infrared intensity, Raman activity and Raman intensities of 7-Oxime by using B3LYP method with 6-311++G(d,p) basis set has been detailed in Table 3.

**Table 3.** Experimental and calculated (unscaled and scaled) B3LYP/6-311G++(d,p) level vibrational frequencies ( $\text{cm}^{-1}$ ) and their assignments to the title molecule

No.	Exp. frequencies		B3LYP/6-311++G(d,p)					Characterization of normal modes with PED (%)
	FT-IR	FT-Raman	Unscaled	Scaled	$f^{\text{IR}}$	$S$	$f^{\text{Ra}}$	
1	3297 (s)	-	3827	3666	169.2	210.5	53.0	$\nu$ OH Oxime (100)
2	-	-	3367	3226	318.3	71.3	28.0	$\nu$ OH Phenol (99)

3	3084 (w)	3071 (vw)	3207	3072	3.1	190.0	87.1	$\nu_s$ CH R2 (99)
4	-	-	3205	3071	0.6	126.9	58.3	$\nu$ CH R1 (99)
5	-	-	3190	3056	2.2	54.7	25.5	$\nu_{as}$ CH R2 (99)
6	-	3017 (vw)	3154	3022	4.9	32.3	15.6	$\nu$ CH Oxime (100)
7	2998 (w)	2979 (vw)	3122	2991	16.9	81.8	40.7	$\nu_{as}$ CH <sub>3</sub> (99)
8	-	-	3080	2950	8.4	69.8	36.1	$\nu_{as}$ HCH Methyl (100)
9	-	-	3030	2903	10.0	217.9	118.3	$\nu_s$ CH <sub>3</sub> (99)
10	1692 (vs)	1690 (s)	1806	1731	746.8	153.0	281.5	$\nu$ C=O lactone (83)
11	1616 (m)	1625 (m)	1679	1650	54.8	142.4	301.3	$\nu$ CN Oxime (68)
12	-	-	1665	1636	88.7	213.5	459.0	$\nu$ CC (64)
13	1588 (s)	1594 (vs)	1626	1598	364.8	245.2	550.7	$\nu$ CC (51)
14	-	-	1616	1588	46.3	137.1	311.3	$\nu$ CC (53)
15	-	1499 (w)	1519	1493	42.0	37.7	95.7	$\delta$ CCH Scissoring R2 (32)+ $\nu$ CC (19) + $\nu$ O1-C2 lactone (10)
16	1470 (m)	1462 (m)	1492	1466	5.6	19.8	52.0	$\delta_{as}$ CH <sub>3</sub> deformation (82)
17	-	-	1484	1459	10.8	9.2	24.4	$\delta_{as}$ CH <sub>3</sub> deformation (98)
18	-	-	1478	1453	44.0	56.4	150.2	$\nu$ CC (30)+ $\delta$ C-OH Phenol (16)
19	-	1410 (vw)	1454	1429	9.7	42.1	115.4	$\delta$ HCN Oxime Scissoring (67)+ $\nu$ CC (10)
20	1393 (m)	1389 (m)	1418	1394	51.1	27.7	79.4	$\delta_s$ CH <sub>3</sub> deformation, umbrella (70)
21	-	-	1409	1385	168.4	118.3	342.5	$\nu$ CC (15) + $\delta_s$ CH <sub>3</sub> deformation, umbrella (14)
22	1366 (m)	1369 (s)	1398	1374	11.5	33.7	99.0	$\delta$ C-OH Phenol (32) + $\nu$ CC (14)
23	-	1337 (m)	1363	1340	18.0	171.8	525.9	$\nu$ C <sub>10</sub> -O <sub>1</sub> lactone (58)
24	1302 (m)	1286 (m)	1321	1298	175.9	33.9	109.4	$\nu$ C-O Phenol (51) + $\delta$ C-OH Phenol Rocking (11)
25	-	1253 (vw)	1293	1271	64.2	35.5	118.7	$\delta$ HON Oxime (72) + $\nu$ CN Oxime (12)
26	1275 (s)	1231 (vw)	1266	1244	1.9	1.3	4.6	$\delta$ HCC R2 (40)
27	1225 (m)	1192 (vw)	1246	1225	66.2	13.6	48.2	$\delta$ HCC R1 (37) + $\nu$ C-O Phenol (13)
28	1190 (s)	1178 (vs)	1209	1189	28.2	15.7	58.4	$\delta$ HCC R2 (38) + $\nu$ CC Oxime (13) + $\nu$ CC (11)
29	-	1139 (vw)	1164	1144	42.8	94.3	373.9	$\nu$ C <sub>10</sub> -O <sub>1</sub> lactone (23) + $\delta$ HCC R2 (29)
30	-	-	1143	1123	0.6	24.1	98.5	$\nu$ CC R1(44)
31	1080 (m)	1082 (vw)	1088	1070	91.7	19.4	85.5	$\nu_{as}$ C <sub>10</sub> -O <sub>1</sub> -C <sub>2</sub> lactone (62)
32	-	1030 (vw)	1058	1040	1.9	0.5	2.1	$\delta$ CH <sub>3</sub> Rocking (84)
33	1022 (m)	997 (vw)	1031	1014	107.4	4.4	21.1	$\delta$ CH <sub>3</sub> Rocking (57) + $\nu$ N-O Oxime (21)
34	993 (m)	-	1005	988	110.3	13.4	66.5	$\nu$ N-O Oxime (58) + $\delta$ CH <sub>3</sub> Rocking (14)
35	-	-	994	977	10.8	3.3	16.9	$\tau$ HCNO Oxime (87)
36	947 (w)	951 (vw)	963	947	0.3	0.4	2.0	$\tau$ HCCH R2 (90)
37	-	-	948	932	40.6	9.3	50.6	$\nu$ CC R1, R2 (41) + $\delta$ CCN Oxime Rocking (10)
38	851 (m)	857 (vw)	871	856	36.1	0.9	5.9	$\gamma$ lactone (88)
39	-	-	843	828	58.7	8.4	54.5	$\nu$ O <sub>1</sub> -C <sub>2</sub> lactone (44) + $\gamma$ HCC R2 (14)
40	-	807 (vw)	831	817	9.1	0.2	1.4	$\tau$ HCC-O Phenol R2 (92)
41	-	-	804	791	0.7	4.1	28.6	$\nu$ C <sub>10</sub> -O <sub>1</sub> lactone (50)
42	-	764 (w)	763	750	38.3	9.2	69.2	$\delta$ CCC R1, R2 deformation ring (55)
43	737 (m)	-	744	731	15.7	0.3	2.4	$\tau_s$ CC-OH Phenol (78) + $\tau$ OCO (12)
44	-	705 (w)	734	721	112.9	0.8	6.0	$\tau_{as}$ CC-OH Phenol (79)
45	-	-	708	696	9.9	8.6	71.6	$\nu_s$ C <sub>10</sub> -O <sub>1</sub> -C <sub>2</sub> lactone (11) + $\gamma$ HCC R2 (48)
46	-	-	706	694	0.0	0.4	3.7	$\gamma$ lactone deformation, umbrella (78)
47	-	-	649	638	3.9	0.1	0.8	$\tau$ OC-CC Phenol-Oxime (81)
48	602 (w)	603 (m)	606	596	15.2	2.1	22.4	$\delta$ CC-C Scissoring R1-CH <sub>3</sub> (74)
49	-	572 (m)	574	565	0.8	0.8	9.3	$\tau$ CC-C <sub>10</sub> O <sub>1</sub> Oxime-lactone (77)
50	-	544 (vs)	543	533	4.7	16.9	206.3	$\gamma$ CCH R2 (21) + $\delta$ CCC R1 deformation ring (45)
51	-	521 (s)	513	504	14.9	1.7	22.6	$\delta$ CCO Phenol Scissoring (64)
52	-	508 (s)	511	503	2.7	1.0	13.9	$\tau$ CCCC R1, R2 (84)
53	451 (w)	452 (s)	452	444	9.6	6.9	110.9	$\delta$ C <sub>3</sub> -C <sub>2</sub> O <sub>1</sub> lactone (72)
54	-	419 (s)	434	427	3.0	11.5	195.6	$\delta$ CC-O Phenol Scissoring (55)
55	-	-	412	405	12.1	9.0	164.3	$\delta$ C-CN Oxime (70)
56	-	384 (s)	381	375	3.5	1.5	31.3	$\tau_s$ HONC Oxime (86)
57	-	-	357	351	111.9	0.2	4.0	$\tau_{as}$ CC-CC Oxime (82)
58	-	311 (s)	349	343	1.2	3.1	72.8	$\gamma$ CCC R2, R1 (33) + $\nu$ C-C Oxime (24)
59	-	-	296	291	0.6	4.9	150.5	$\delta$ C-CN Oxime Rocking (62)
60	-	-	283	278	2.7	0.2	6.4	$\tau$ CCCC R2, R1 (77)
61	-	241 (s)	255	250	1.4	0.3	12.5	$\delta$ C-CN Oxime Rocking (62)
62	-	-	220	216	1.8	1.2	58.2	$\tau$ C <sub>2</sub> O <sub>1</sub> -C <sub>10</sub> C <sub>5</sub> lactone (81)
63	-	191 (vs)	203	200	0.2	0.6	33.2	$\tau$ CH <sub>3</sub> (88)
64	-	-	159	156	0.0	0.4	32.8	$\tau$ CH <sub>3</sub> (84)
65	-	-	152	149	5.0	1.6	149.7	$\tau$ C-C-CN Phenol-Oxime (78)
66	-	132 (m)	133	130	2.7	4.0	468.5	$\delta$ CC-C Oxime Rocking (77)
67	-	-	119	117	0.3	0.4	63.1	$\tau$ OC-C-C Phenol-Oxime (74)
68	-	-	96	95	0.0	0.3	53.2	$\tau$ C <sub>2</sub> O <sub>1</sub> -C <sub>10</sub> C <sub>9</sub> lactone (80)
69	-	-	55	54	3.5	0.0	14.2	$\tau$ CCC-C R1-Methyl (83)

Freq<sub>Theo</sub> = 1.0578 Freq<sub>Exp</sub> - 65.632

R<sup>2</sup> = 0.9931

RMSD=81.80261

<sup>a</sup> s: strong; vs: very strong; m: medium; w: weak; vw: very weak.

<sup>b</sup> I<sup>R</sup>: Infrared intensity; S: Raman activity; I<sup>Ra</sup>: Raman intensity.

<sup>c</sup>  $\nu$ : stretching;  $\delta$ : in-plane bending;  $\gamma$ : out-of-plane bending;  $\tau$ : torsion; s: symmetry; as: asymmetry; R1: lactone ring; R2: aromatic ring.

<sup>d</sup> The linear regression between theoretical and experimental frequencies was shown by the formula "Freq<sub>Theo</sub> = 1.0578 Freq<sub>Exp</sub> - 65.632" (R<sup>2</sup> = 0.9931 and RMSD=81.80261) which Freq<sub>Theo</sub>, Freq<sub>Exp</sub>, R<sup>2</sup> and RMSD are theoretical frequencies, experimental frequencies, correlation coefficient and Root Mean Square Deviation, respectively.

The observed and calculated frequencies of the FT-IR and FT-Raman spectra have been shown in Fig. 5. In addition, the specific assignment of each frequency was performed via potential energy distribution (PED) by using VEDA program [21]. Also, the normal mode animations were built by GaussView program [19] to support the accuracy of vibrational assignments.

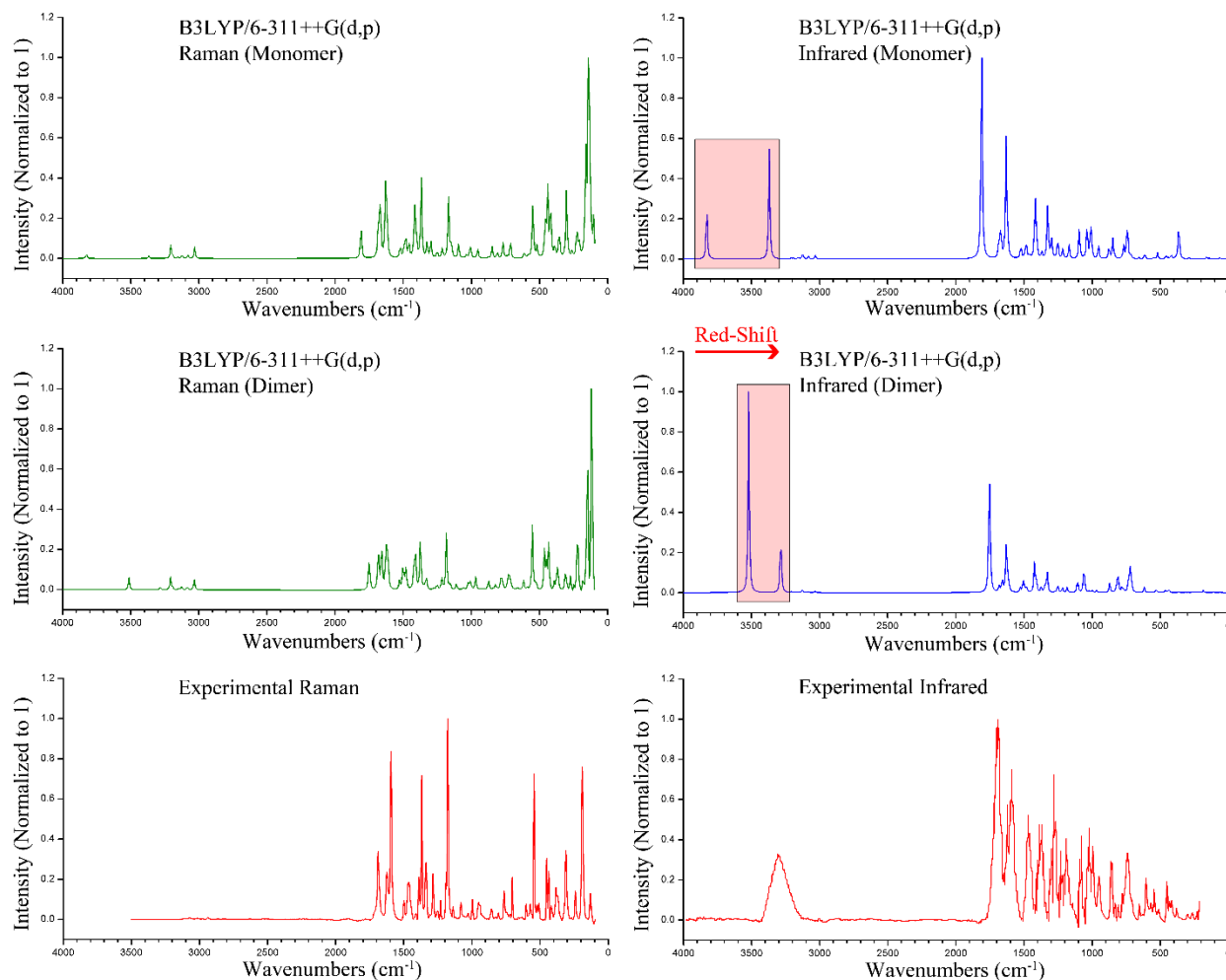


**Fig. 5.** The comparison of experimental and calculated FT-IR and FT-Raman spectra of 7-oxime

### 3.3.1. O-H vibrations

All three vibrations related to OH groups (stretching, in-plane and out-of-plane bending vibrations) are IR-active while only in-plane and out-of-plane bending modes are Raman-active. These vibrations are the most sensitive ones to the environment and their peaks significantly shift toward the lower frequencies upon the formation of hydrogen bonds. In fact, the strength of the hydrogen bond determines the exact positions of O-H peaks. The stretching vibrations of the free hydroxyl

group, without any hydrogen bond, usually create a strong peak in the region of 3584-3700  $\text{cm}^{-1}$  while these peaks appear with higher intensity and broadness in the region of 3000-3550  $\text{cm}^{-1}$  upon the formation of intermolecular and intramolecular hydrogen bonds [39].

As shown in the FT-IR spectrum of 7-Oxime, the stretching vibrations of the phenolic OH group caused a broad absorption band between 2600 and 3400  $\text{cm}^{-1}$  [40]. The possible reason for the broadness of this peak is the presence of strong intramolecular hydrogen bonds between the hydrogen of the phenolic OH group ( $\text{O}_{13}\text{-H}_{23}$ ) and the nitrogen atom of the oxime group. The computed wavenumber related to the stretching vibrations of this mode was obtained 3226  $\text{cm}^{-1}$  (mode No. 2) by B3LYP/6-311++G(d,p) method with PED contribution of 99%.

Also, a relatively strong band was observed at 3297  $\text{cm}^{-1}$  which can be assigned to the O-H stretching vibrations of the oxime group while the computed value of this O-H stretching frequency was 3666  $\text{cm}^{-1}$  (mode No. 1) with PED contribution of 100%. The possible reason for the deviation of 300  $\text{cm}^{-1}$  is due to the presence of strong intermolecular hydrogen bonds [41]. The appearance of the red shift in the O-H stretching vibration of the oxime and phenolic group (at the dimer form) clearly been shown in Fig. 5. This hypothesis was proved by some MEP calculations which were applied to find the possible sites of intermolecular hydrogen bond. In addition, NBO analysis confirmed the presence of some strong hydrogen bonds between the monomers in the dimer form.

The in-plane bending vibrations of O-H generally appeared in the region of 1150-1250  $\text{cm}^{-1}$ . Unlike the stretching and out-of-plane bending deformation frequencies, the position of these vibrations were not affected by the formation of hydrogen bonds [42]. Normally, the O-H in-plane bending vibrations appear in the same region with C-H in-plane bending vibrations and C-C stretching vibrations. Herein, the medium band observed at 1366  $\text{cm}^{-1}$  in the FT-IR spectrum and the strong band observed at 1369  $\text{cm}^{-1}$  in the FT-Raman spectrum were related to the in-plane bending vibrations of the phenolic O-H groups. Also, in the FT-Raman spectrum, the very weak band appeared at 1253  $\text{cm}^{-1}$  was assigned to the O-H in-plane bending vibrations of the oxime group. Moreover, there was a good agreement between the experimental and the computational data as the computed wavenumbers were obtained at 1374  $\text{cm}^{-1}$  (mode No. 22) and 1271  $\text{cm}^{-1}$  (mode No. 25) with PED contribution of 32% and 72 % (by B3LYP/6-311++G(d,p) method) for the phenolic OH in-plane bending vibrations and the O-H in-plane bending vibrations of the oxime group, respectively.

The out-of-plane bending vibrations of O-H usually appear as a broad band in the region of 517–710  $\text{cm}^{-1}$ , in both intermolecular and intramolecular association [43]. In fact, the strength of the hydrogen bond is the determining factor for the position of this band. In other words, the band shifts toward higher wavenumbers by increasing the strength of the hydrogen bond. According to our experimental data, the phenolic O-H out-of-plane bending vibrations created the weak bands at 705  $\text{cm}^{-1}$  and 737  $\text{cm}^{-1}$  in the FT-Raman and FT-IR spectra, respectively. The corresponding computed wavenumbers were calculated by B3LYP/6-311++G(d,p) method and obtained to be 721  $\text{cm}^{-1}$  (mode No. 44) and 731  $\text{cm}^{-1}$  (mode No. 43) with PED contribution of 79% and 78%, respectively. The generated results indicated a good correlation between the experimental and the computational data.

However, the O-H out-of plane bending vibrations of the oxime group appeared below 500  $\text{cm}^{-1}$  due to the formation of intermolecular and intramolecular hydrogen bonds. Also, the strong band observed at 384  $\text{cm}^{-1}$  (in the FT-Raman spectrum) was related to the O-H out-of-plane bending vibrations. Finally, the corresponding computed wavenumber was 375  $\text{cm}^{-1}$  (mode No. 56) with PED contribution of 86%; and confirmed the agreement between the experimental and the theoretical data.

### 3.3.2. C-H and CH<sub>3</sub> vibrations

In 7-Oxime, there are three C-H bonds related to the aromatic structure and one C-H bond related to the oxime group so we can expect four C-H stretching, C-H in-plane and C-H out-of plane bending vibrations corresponding to C<sub>3</sub>-H<sub>17</sub>, C<sub>6</sub>-H<sub>21</sub>, C<sub>7</sub>-H<sub>22</sub> (aromatic rings) and C<sub>14</sub>-H<sub>24</sub> (oxime group). The characteristic region for the aromatic C-H stretching vibrations is between 3000-3100  $\text{cm}^{-1}$  [44-46] and the nature of the substituents only slightly affect the position of these peaks.

The weak band appeared at 3084  $\text{cm}^{-1}$  in the FT-IR spectrum of our compound was assigned to the aromatic C-H stretching vibrations. Also, the other very weak bands observed at 3071 and 3017  $\text{cm}^{-1}$  in the FT-Raman spectrum were related to the stretching vibrations of aromatic C-H as well as C-H of the oxime moiety, respectively. The calculated frequencies for these vibrations were obtained 3072, 3071, 3056 (aromatic groups) and 3022  $\text{cm}^{-1}$  (oxime group) (mode Nos. 3-6) by B3LYP/6-311++G(d,p) method.

The results of the PED column displayed that these modes were pure stretching modes and their contribution was 99%, respectively. Our results for these analysis is fully in accordance with the

previous reports [13, 47]. The results showed that the C-H stretching vibrations were not affected by the substitution and also all of the mentioned vibrations were observed in the expected range.

The in-plane and out-of-plane bending vibrations of aromatic C-H group generally create peaks in the range of 1050-1400  $\text{cm}^{-1}$  and 675-1000  $\text{cm}^{-1}$ , respectively [45, 46]. In our molecule, the bands recorded at 1275 (strong), 1225 (medium) and 1190 (strong)  $\text{cm}^{-1}$  in the FT-IR spectrum; plus the bands appeared at 1499 (weak), 1231 (very weak), 1192 (very weak), 1178 (very strong) and 1139 (very weak)  $\text{cm}^{-1}$  in the FT-Raman spectrum belonged to the aromatic C-H in-plane bending vibrations of the title compound. The corresponding computed frequencies were 1493, 1244, 1225, 1189 and 1144  $\text{cm}^{-1}$  (mode Nos. 15, 26-29) and the PED corresponding to these modes was a mixed mode of 29-40%. Also, the very weak band observed at 1410  $\text{cm}^{-1}$  in the FT-Raman spectrum was related to the in-plane bending vibrations of the C-H group of the oxime moiety while the calculated frequency of this vibration was seen at 1429  $\text{cm}^{-1}$  (mode No.19), with PED contribution of 67%.

Also, the weak band at 947  $\text{cm}^{-1}$  in the FT-IR spectrum and the very weak bands at 951 and 807  $\text{cm}^{-1}$  in the FT-Raman spectrum were related to the out-of-plane bending vibrations of the aromatic C-H groups. Consequently, the computed frequencies for these modes were 947 and 817  $\text{cm}^{-1}$  (mode Nos. 36 and 40) with PED contributions of 90% and 92%, respectively, and these results showed a good agreement with the experimental data. The out-of-plane bending vibrations related to the C-H of the oxime group could not be recognized in the experimental FT-IR and FT-Raman spectra. However, their computed frequencies are detailed in Table 3.

In order to evaluate the peaks related to the vibrations of  $\text{CH}_3$  group, we should know that there are nine fundamental vibrations associated to each  $\text{CH}_3$  group: three stretching modes, three bending modes, two rocking modes and a single torsional mode [48]. Aromatic C-H stretching vibrations appear in the range of 3000-3100  $\text{cm}^{-1}$  while C-H asymmetric and symmetric stretching modes of  $\text{CH}_3$  group normally appear in lower frequencies (at the region of 2850-3000  $\text{cm}^{-1}$ ) [45, 46].

The asymmetric stretching frequencies of the  $\text{CH}_3$  group were recorded at 2998  $\text{cm}^{-1}$  (as a weak band) in the FT-IR spectrum and 2979  $\text{cm}^{-1}$  (as a very weak band) in the FT-Raman spectrum. The calculated frequency of this mode was 2991  $\text{cm}^{-1}$  (mode No. 7) with PED contribution of 99%. In addition, the symmetric stretching vibrations of this group were not detectable in the experimental

FT-IR and FT-Raman spectra. However, the calculated frequency related to this mode was 2950  $\text{cm}^{-1}$  (mode No. 8) with PED contribution of 100% (Table 3).

The asymmetric and symmetric bending vibrations of the  $\text{CH}_3$  groups normally appear in the range of 1410-1465 and 1370-1390  $\text{cm}^{-1}$ , respectively [46, 49, 50]. In the spectra of the title compound, the medium bands appeared at 1470  $\text{cm}^{-1}$  (in the FT-IR spectrum) and 1462  $\text{cm}^{-1}$  (in the FT-Raman spectrum) were related to the  $\text{CH}_3$  asymmetric bending (deformation) vibrations. The computed frequency for this mode was calculated to be equal with 1466  $\text{cm}^{-1}$  (mode No. 16) with PED contribution of 82%. Also, the  $\text{CH}_3$  symmetric bending (deformation, umbrella) vibrations created the medium bands at 1393  $\text{cm}^{-1}$  in the FT-IR spectrum and 1389  $\text{cm}^{-1}$  in the FT-Raman spectrum. The calculated frequency for this mode was 1394  $\text{cm}^{-1}$  (mode No. 20) with PED contribution of 70%, and showed a good agreement with the experimental value.

The rocking modes of methyl groups usually create the bands in the region of 1010-1070  $\text{cm}^{-1}$  [45]. Herein, the medium band at 1022  $\text{cm}^{-1}$  in the FT-IR spectrum and the very weak bands at 1030  $\text{cm}^{-1}$  and 997  $\text{cm}^{-1}$  in the FT-Raman spectrum were due to the  $\text{CH}_3$  rocking vibrations. The calculated frequencies for the  $\text{CH}_3$  rocking vibrations were equal with 1014 and 1040  $\text{cm}^{-1}$  (mode No. 32, 33) with PED contributions of 84% and 57%, respectively.

The torsional modes related to  $\text{CH}_3$  groups generally appear in low-frequency regions. Govindarajan *et al.* [51] calculated the normal modes of the  $\text{CH}_3$  out-of-plane motions (torsional  $\text{CH}_3$  modes) and they reported that these signals appeared below 250  $\text{cm}^{-1}$ . According to our results, the  $\text{CH}_3$  torsional modes created a very strong band at 191  $\text{cm}^{-1}$  in the FT-Raman spectrum. This value showed a good correlation with the corresponding computed wavenumber (200  $\text{cm}^{-1}$  (mode No. 63) with PED contribution of 88%). Our results indicated that the computational outputs for the vibrations of the methyl group were in good agreement with experimental results.

### 3.3.3. C-O and C=O (lactone) vibrations

The stretching frequencies of carbonyl groups have been extensively studied by infrared spectroscopy because almost all peaks related to these groups are very intense and narrow, and they appeared in the range of 1600-1800  $\text{cm}^{-1}$  [46]. Coumarin derivatives have two characteristic

bands arising from C=O and C-O (lactone) stretching vibrations [52]. The positions of these bands are very clear and sensitive to the infrared environment [52]. The stretching vibrations of C=O groups in the coumarin ring occur at higher frequencies than that of normal C=O groups.

In our molecule, the stretching vibrations corresponding to the carbonyl group in the coumarin were observed as a very strong band at  $1692\text{ cm}^{-1}$  in the FT-IR spectrum and a strong band at  $1690\text{ cm}^{-1}$  in the FT-Raman spectrum. The calculated C=O stretching frequency was appeared at  $1731\text{ cm}^{-1}$  (mode No. 10) with PED contribution of 83%. The deviation (about  $40\text{ cm}^{-1}$ ) observed between the experimental and the computational results were probably caused by the intermolecular hydrogen bonds. This assumption was confirmed by using the results of NBO analysis in the dimer form.

In addition, the out-of-plane bending mode of the C=O group was appeared as a medium band at  $851\text{ cm}^{-1}$  in the FT-IR spectrum and a very weak band at  $857\text{ cm}^{-1}$  in the FT-Raman spectrum. The calculated wavenumber related to this mode was  $856\text{ cm}^{-1}$  (mode No. 38) with PED contribution of 88%. This confirmed the link between experimental and theoretical calculations.

The peaks related to C-O stretching vibrations usually appear in the range of  $1050\text{-}1400\text{ cm}^{-1}$  [51-52]. The C<sub>10</sub>-O<sub>1</sub> (in the lactone group) stretching vibrations appeared the medium band at  $1337\text{ cm}^{-1}$  in the FT-Raman spectrum. The calculated frequency for this mode (appeared at  $1340\text{ cm}^{-1}$  (mode No. 23) with PED contribution of 58%) was in good agreement with the experimental data. Also, the asymmetric stretching vibrations of C<sub>10</sub>-O<sub>1</sub>-C<sub>2</sub> (in the lactone group) appeared the medium band at  $1080\text{ cm}^{-1}$  in the FT-IR spectrum and the very weak band at  $1082\text{ cm}^{-1}$  in the FT-Raman spectrum. The corresponding calculated wavenumber for this mode created a band at  $1070\text{ cm}^{-1}$  (mode No. 31) with PED contribution of 62% which was in good agreement with the experimental data.

#### 3.3.4. C=N and N-O vibrations

The bands related to the C=N stretching vibrations of oxime groups usually appear in the range of  $1610\text{-}1690\text{ cm}^{-1}$  [40, 53]. In the previous studies [54], the peak observed at  $1625\text{ cm}^{-1}$  in the FT-IR spectrum was assigned to the C=N stretching vibrations of an oxime moiety. Herein, the medium bands at  $1616\text{ cm}^{-1}$  in the FT-IR spectrum and  $1625\text{ cm}^{-1}$  in the FT-Raman spectrum were ascribed to the C=N stretching vibrations of the oxime group (C<sub>14</sub>=N<sub>15</sub>). According to our results, the frequency of this vibrational mode was  $1650\text{ cm}^{-1}$  (mode No. 11) with PED contribution of

68%. Also, the C=N in-plane bending vibrations of the oxime group led to a strong band at 241  $\text{cm}^{-1}$  in the FT-Raman spectrum and it showed a good agreement with the corresponding computed frequency ( 250  $\text{cm}^{-1}$  (mode No. 61) with PED contribution of 62%).

The characteristic frequencies of the N-O group of oxime moieties are not usually affected by substituents. In general, the stretching vibrations of N-O in oxime groups which are bonded to aromatic compounds cause an absorption band at 960  $\text{cm}^{-1}$  [55]. Herein, the N<sub>15</sub>-O<sub>16</sub> stretching vibrations were observed as a medium band at 993  $\text{cm}^{-1}$  in the FT-IR spectrum. The computed frequency related to this mode was 988  $\text{cm}^{-1}$  (mode No. 34) with PED contribution of 58% and it was in good agreement with the experimental results. Consequently, the results that we reported for the vibrations of C=N and N-O groups of our compound were in a good agreement with the spectral data reported for the oxime derivatives in the literature [56-58].

### 3.3.5. Ring vibrations

In the vibrational spectra of benzene and its derivatives, the ring stretching vibrations are very prominent [59]. Varsanyi *et al* [59] reported that rings vibrations appear at five regions of 1590-1625, 1550-1575, 1470-1540, 1430-1465 and 1280-1380  $\text{cm}^{-1}$  with different intensities.

Also, in saturated lactones, the absorption band related to the C=C adjacent to the -O- usually appears in the region of 1660-1685  $\text{cm}^{-1}$ . In fact, the form of substitutions around the rings can determine the actual position of these modes [60].

Herein, the calculated wavenumber of 1598  $\text{cm}^{-1}$  (mode No. 13) with PED contribution of 51% was assigned to C=C stretching vibrations. These results are in good agreement with the experimental results (recorded as a strong band at 1588  $\text{cm}^{-1}$  in the FT-IR spectrum and a very strong band at 1594  $\text{cm}^{-1}$  in the FT-Raman spectrum).

In addition, a weak band at 764  $\text{cm}^{-1}$  and a very strong band at 544  $\text{cm}^{-1}$  in the FT-Raman spectrum were assigned to the in-plane vibrations of CCC of the rings (deformation). The corresponding computed frequency was obtained to be 750 and 533  $\text{cm}^{-1}$  (mode No. 42, 50) for this mode with PED contribution of 55% and 45%. A good agreement was observed between the experimental and computational frequencies related to these vibrations. Also, the computed wavenumbers at 503 and 343  $\text{cm}^{-1}$  (mode Nos. 52, 58); with PED contributions of 84% and 33% were related to the torsional and out-of-plane vibrations of CCCC and CCC in the rings, respectively. In the experimental FT-Raman spectrum, the strong bands at 508 and 311  $\text{cm}^{-1}$  were

assigned to these frequencies, respectively. Fig. S.2 depicts the relationship between the experimental and computed (by DFT/B3LYP/6-311++G(d,p)) frequencies of these vibrations. The quality of the correlation in frequencies is judged by the correlation coefficient ( $R^2=0.9931$ ) and the Root Mean Square Deviation (RMSD=81.80261). Besides, there is a linear regression as  $\text{Freq}_{\text{Theo}} = 1.0578 \text{ Freq}_{\text{Exp}} - 65.632$  between the experimental and the calculated frequencies of these vibrations.

### 3.4. NMR spectral analysis

The GIAO method [11, 25] was applied to calculate  $^1\text{H}$  NMR chemical shifts of the title compound. The isotropic shielding values ( $\sigma$ ) were used to calculate the isotropic chemical shifts  $\delta$  ( $\delta^{\text{X}} = \sigma^{\text{TMS}} - \sigma^{\text{X}}$ ) with respect to tetramethylsilane (TMS) as a reference molecule considered at the same theoretical level (DFT/B3LYP/6-311++G(d,p)). The solvent effect of DMSO on the spectra was modeled using the conductor-like polarizable continuum model (CPCM) with dielectric constant  $\epsilon = 46.68$  on the fully optimized geometry [61-64]. Fig. 4 shows the numbering system used for NMR calculations of the monomer and dimer form. Also, the experimental  $^1\text{H}$  and  $^{13}\text{C}$  NMR spectra have been shown in Figs. 6 and 7, respectively.

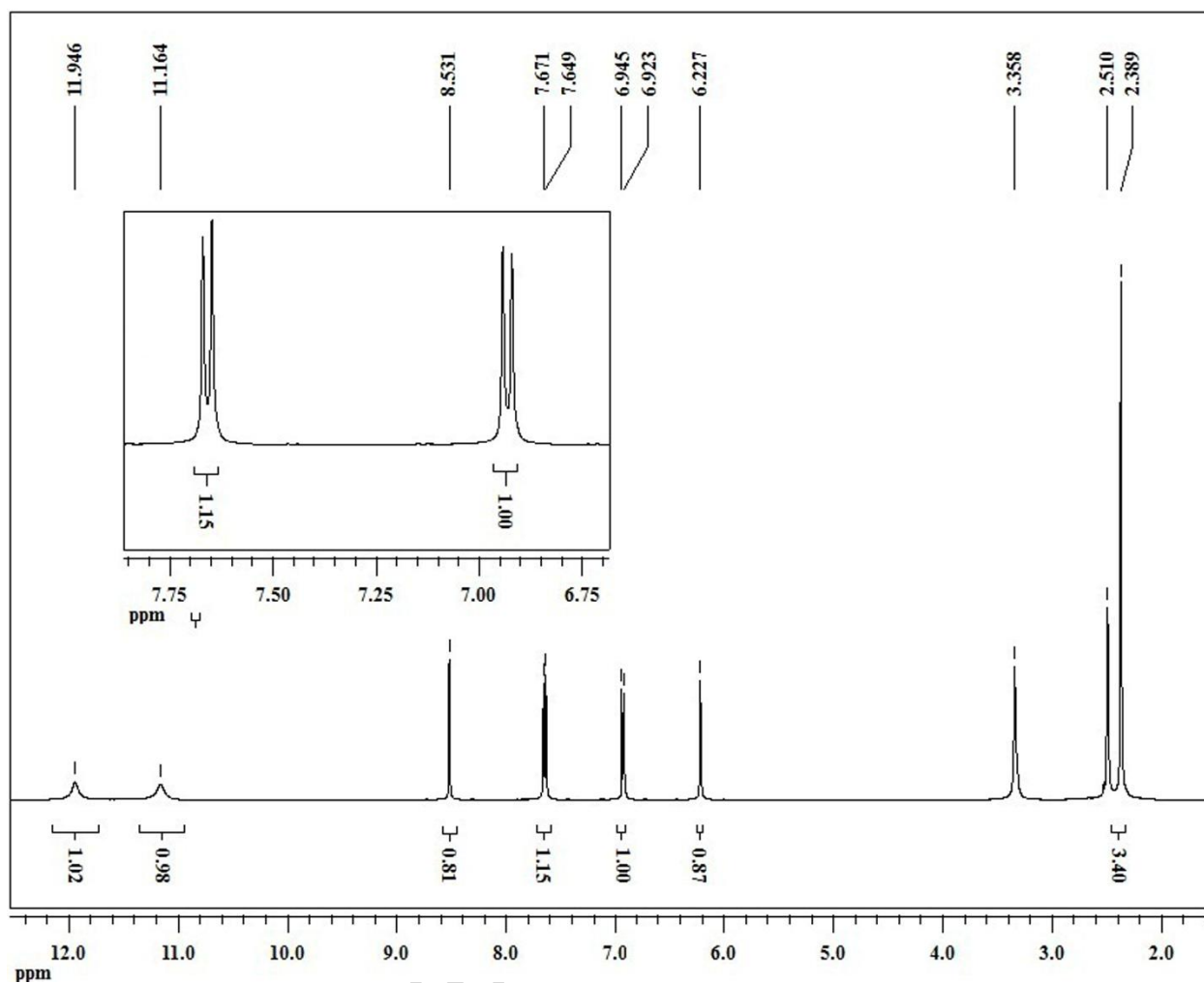


Fig. 6.  $^1\text{H}$  NMR spectrum of 7-Oxime

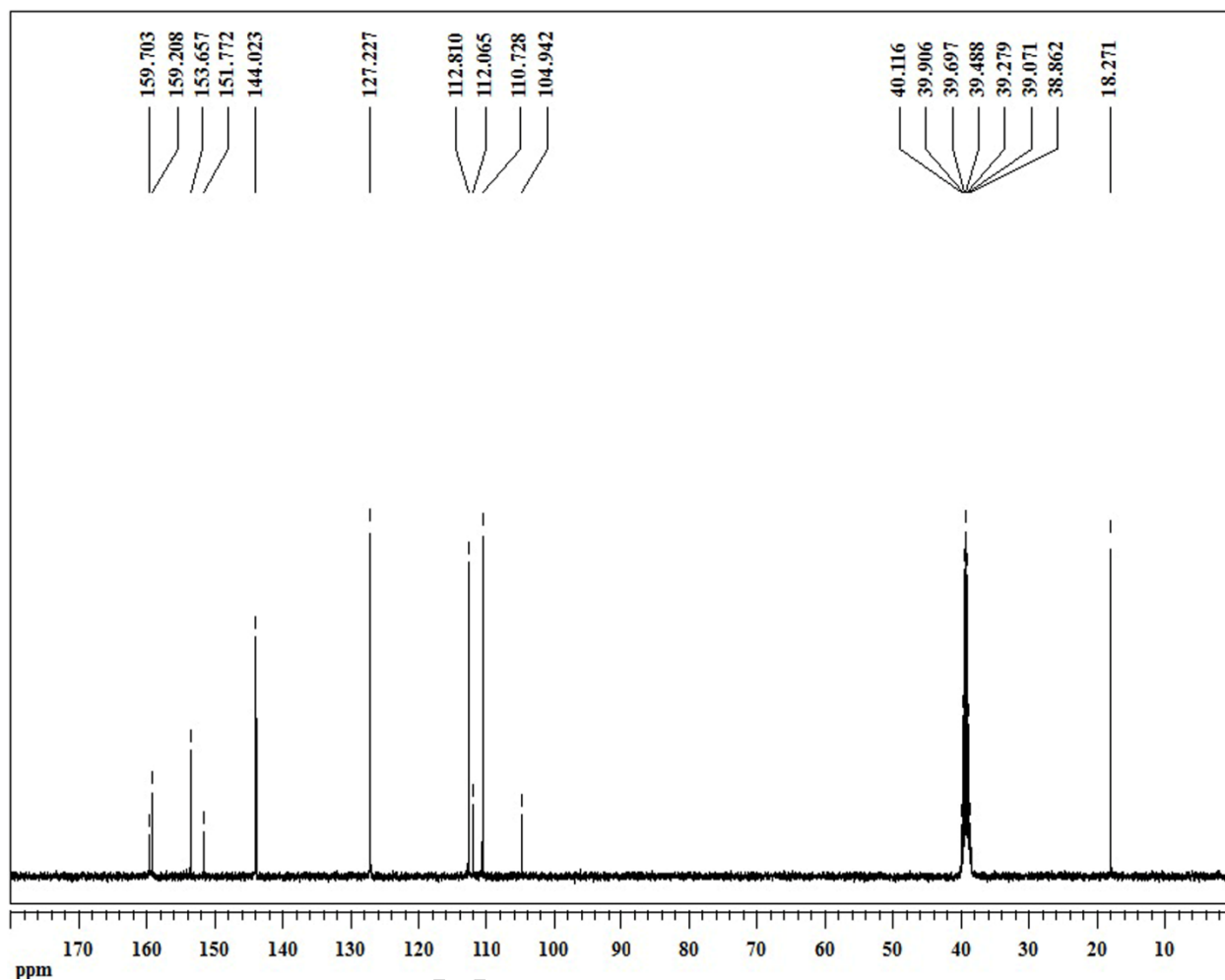


Fig. 7.  $^{13}\text{C}$  NMR spectrum of 7-Oxime

The calculated values for  $^1\text{H}$ ,  $^{13}\text{C}$  NMR chemical shifts (for the monomer and dimer forms) were obtained in DMSO and the vacuum. In addition, the corresponding experimental spectra were obtained in DMSO. Both of the obtained experimental ( $\delta_{\text{Exp}}$ ) and the calculated ( $\delta_{\text{Calc}}$ ) values have been summarized in Table 4.

**Table 4.** Calculated ( $\delta_{\text{Theo}}$ ) (calculated by B3LYP method with 6-311++G(d,p) basis set) and experimental ( $\delta_{\text{Exp}}$ )  $^1\text{H}$  and  $^{13}\text{C}$  NMR chemical shifts for the monomer and dimer form of the title molecule

Atom	Exp.	Monomer				Dimer			
		Gas	$\Delta\delta^a$	DMSO	$\Delta\delta^a$	Gas	$\Delta\delta^a$	DMSO	$\Delta\delta^a$
H(17)	6.227	6.102	0.126	6.315	-0.088	6.016	0.211	6.570	-0.343
H(18)	2.510	2.427	0.083	2.620	-0.110	2.440	0.070	2.656	-0.146
H(19)	2.510	1.997	0.513	2.181	0.329	1.999	0.511	2.248	0.262
H(20)	2.510	2.427	0.083	2.620	-0.110	2.440	0.070	2.656	-0.146
H(21)	7.660	7.427	0.233	7.827	-0.167	7.409	0.251	8.060	-0.400
H(22)	6.934	6.938	-0.004	7.132	-0.198	7.027	-0.093	7.563	-0.629
H(23)	11.164	10.687	0.477	11.035	0.129	11.345	-0.181	10.994	0.170
H(24)	8.531	9.406	-0.874	9.335	-0.804	9.874	-1.343	9.833	-1.302
H(25)	11.946	6.347	5.600	7.132	4.814	10.867	1.079	10.994	0.952
$\delta_{\text{Theo}} = 0.737\delta_{\text{Exp}} + 1.054$		$R^2 = 0.729$		RMSD = 1.906		MAD = 0.888		Monomer (Gas phase)	
$\delta_{\text{Theo}} = 0.772\delta_{\text{Exp}} + 1.098$		$R^2 = 0.785$		RMSD = 1.635		MAD = 0.750		Monomer (DMSO)	
$\delta_{\text{Theo}} = 1.001\delta_{\text{Exp}} - 0.076$		$R^2 = 0.969$		RMSD = 0.614		MAD = 0.423		Dimer (Gas phase)	
$\delta_{\text{Theo}} = 0.970\delta_{\text{Exp}} + 0.371$		$R^2 = 0.970$		RMSD = 0.616		MAD = 0.483		Dimer (DMSO)	
C(2)	153.657	162.904	-9.247	168.526	-14.869	167.591	-13.934	171.320	-17.663
C(3)	110.728	116.801	-6.073	115.878	-5.150	113.904	-3.176	114.148	-3.420
C(4)	151.772	158.901	-7.129	166.073	-14.301	163.349	-11.577	169.341	-17.569
C(5)	112.065	117.339	-5.274	119.280	-7.215	117.522	-5.457	120.071	-8.006
C(6)	127.227	133.058	-5.831	136.292	-9.065	130.797	-3.570	135.654	-8.427
C(7)	112.810	117.892	-5.082	119.432	-6.622	119.320	-6.510	121.205	-8.395
C(8)	159.703	170.916	-11.213	171.209	-11.506	171.757	-12.054	171.603	-11.900
C(9)	104.942	109.721	-4.779	110.152	-5.210	113.020	-8.078	112.254	-7.312
C(10)	144.023	162.603	-18.580	162.091	-18.068	160.138	-16.115	160.593	-16.570
C(12)	18.271	21.8773	-3.606	22.5758	-4.305	20.756	-2.485	21.4811	-3.210
C(14)	159.208	155.647	3.561	155.469	3.739	155.924	3.284	159.003	0.205
$\delta_{\text{Theo}} = 1.032\delta_{\text{Exp}} + 2.723$		$R^2 = 0.984$		RMSD = 8.423		MAD = 7.307		Monomer (Gas phase)	
$\delta_{\text{Theo}} = 1.048\delta_{\text{Exp}} + 2.419$		$R^2 = 0.982$		RMSD = 10.219		MAD = 9.095		Monomer (DMSO)	
$\delta_{\text{Theo}} = 1.051\delta_{\text{Exp}} + 0.873$		$R^2 = 0.984$		RMSD = 9.097		MAD = 7.840		Dimer (Gas phase)	
$\delta_{\text{Theo}} = 1.070\delta_{\text{Exp}} + 0.639$		$R^2 = 0.985$		RMSD = 10.946		MAD = 9.334		Dimer (DMSO)	

$$^a \Delta\delta = \delta_{\text{Exp}} - \delta_{\text{Theo}}$$

The quality of each correlation in NMR data was interpreted by the following parameters: the correlation coefficient ( $R^2$ ), the Root Mean Square Deviation (RMSD) and the Mean Absolute Deviation (MAD). Eq. 2 and Eq. 3 represent the formulas of RMSD and MAD, respectively [65]:

$$\text{RMSD} = \sqrt{\frac{1}{N} \sum_{i=1}^n (\delta_{\text{Exp}} - \delta_{\text{Theo}})^2}, \quad \text{Eq. (2)}$$

$$\text{MAD} = \frac{1}{N} \sum_{i=1}^n |\delta_{\text{Theo}} - \delta_{\text{Exp}}|, \quad \text{Eq. (3)}$$

Where  $N$  is the number of experimental or calculated data,  $\delta_{\text{Exp}}$  denotes experimental chemical shift values and  $\delta_{\text{Theo}}$  gives calculated chemical shift values.

In fact, there is a linear regression ( $\delta_{\text{Calc}} = B \delta_{\text{Exp}} + A$ ) between the experimental and the calculated values (Table 4). Based on the obtained correlations from the dimer and monomer

forms, we can claim that the dimer form of this compound was more accurate than its monomer form in both DMSO and the vacuum so it can be considered as accurate chemistry model for the NMR analysis. Also, the provided results from MEP and NBO supported this issue. On the other hand, MEP results confirmed that the maximum positive region was localized on H<sub>25</sub> atom (in the oxime group) and also the NBO results displayed the presence of some intermolecular hydrogen bonds between each two monomers led to the formation of the dimer forms.

Also, the <sup>1</sup>H chemical shift values (with respect to TMS) were calculated at B3LYP level and they appeared in the range of 1.999–11.345 ppm in the vacuum and 2.248–10.994 ppm in DMSO while the corresponding experimental shifts were observed in the range of 2.510–11.946 ppm. In the experimental spectrum, the characteristic signal at 11.946 ppm was attributed to the proton of hydroxyl group in the oxime moiety (H<sub>25</sub>) while the computational peaks related to this proton appeared in the upfield region in comparison to the experimental one (this peak appeared at 7 ppm in the computational spectrum of the monomer form and 10.30 ppm in that of the dimer form).

The observed difference is interpreted based on the reduction of H<sub>25</sub> electron density by the electronegative oxygen atom (O<sub>16</sub>) and the construction of intermolecular hydrogen bonds between carbonyl group (O<sub>36</sub>) and H<sub>25</sub> in the dimer form. In addition, the experimental signal related to the proton of the other hydroxyl group (H<sub>23</sub>) was appeared at 11.164 ppm and its poor electron density may be due to the presence of the electronegative oxygen atom (O<sub>13</sub>) and the intramolecular hydrogen bond between the nitrogen atom (N<sub>15</sub>) of the oxime group and this proton.

In the experimental <sup>1</sup>H NMR spectrum, the iminic proton of the oxime group (H<sub>24</sub>) appeared as a downfield signal at 8.531 ppm. Also, the aromatic and vinyl protons of the heterocyclic ring appeared at 7.660 (doublet, assigned to H<sub>21</sub>), 6.934 (doublet, assigned to H<sub>22</sub>) and 6.227 (singlet, assigned to H<sub>17</sub>). In addition, the singlet signal appeared at 2.510 ppm corresponded to the protons of the methyl group.

The experimental <sup>13</sup>C chemical shifts of the compound occurred in the range of 18.271–159.703 ppm while the calculated <sup>13</sup>C chemical shift values appeared in the ranges of 21.481–171.603 and 171.757–20.756 ppm in DMSO and the vacuum, respectively. The signals related to the aromatic carbons are usually appeared in the range of 100–200 ppm [66]. The aromatic carbon bonded to the hydroxyl group (C<sub>8</sub>) created the most downfield signal (at 159.703 ppm) probably because of being adjacent to the electronegative oxygen atom. Also, the chemical shift of C<sub>14</sub> (in the oxime

group) was observed in downfield (159.208 ppm) due to the electronegativity of the nitrogen atom. The signal at 153.657 ppm was assigned to the carbonyl of the pyrone ring.

Also, the signals appeared at 112.065, 127.227, 112.810, 104.942 and 144.023 ppm were attributed to the aromatic carbons of C<sub>5</sub>, C<sub>6</sub>, C<sub>7</sub>, C<sub>9</sub> and C<sub>10</sub>, respectively. The aromatic C<sub>10</sub> was observed in downfield in comparison to the other aromatic carbons which may be due to the electronegativity of O<sub>1</sub> in the pyrone ring. Besides, the peak assigned to C<sub>3</sub> (110.728 ppm) appeared in upfield in comparison to C<sub>4</sub> (151.772 ppm) due to the presence of resonance between C<sub>3</sub>=C<sub>4</sub> and C<sub>2</sub>=O<sub>11</sub> which made C<sub>4</sub> more positive than C<sub>3</sub>. In addition, the observed signal at 18.271 ppm was related to the methyl group.

It's obvious from the correlation coefficient ( $R^2$ ) values that there was a good correlation between the experimental and calculated <sup>1</sup>H and <sup>13</sup>C spectra (for the dimer form at B3LYP/6-311++G(d,p) level). The obtained good correlation coefficient proved that we assigned all of the signals correctly. It was obvious from the ( $R^2$ ) values (obtained from the correlation diagrams of the monomer and dimer forms) that the calculated results for the dimer form (both in DMSO and the vacuum) were closer to the experimental results than those of the monomer, proving that the molecules existed in the dimer form. In addition, the correlation coefficient of the dimer form in DMSO was better than that of the dimer form in the vacuum.

In Fig. 8, we have represented a histogram of the deviation and the correlation graphics for both dimer and monomer forms of the title compound in the vacuum and DMSO.

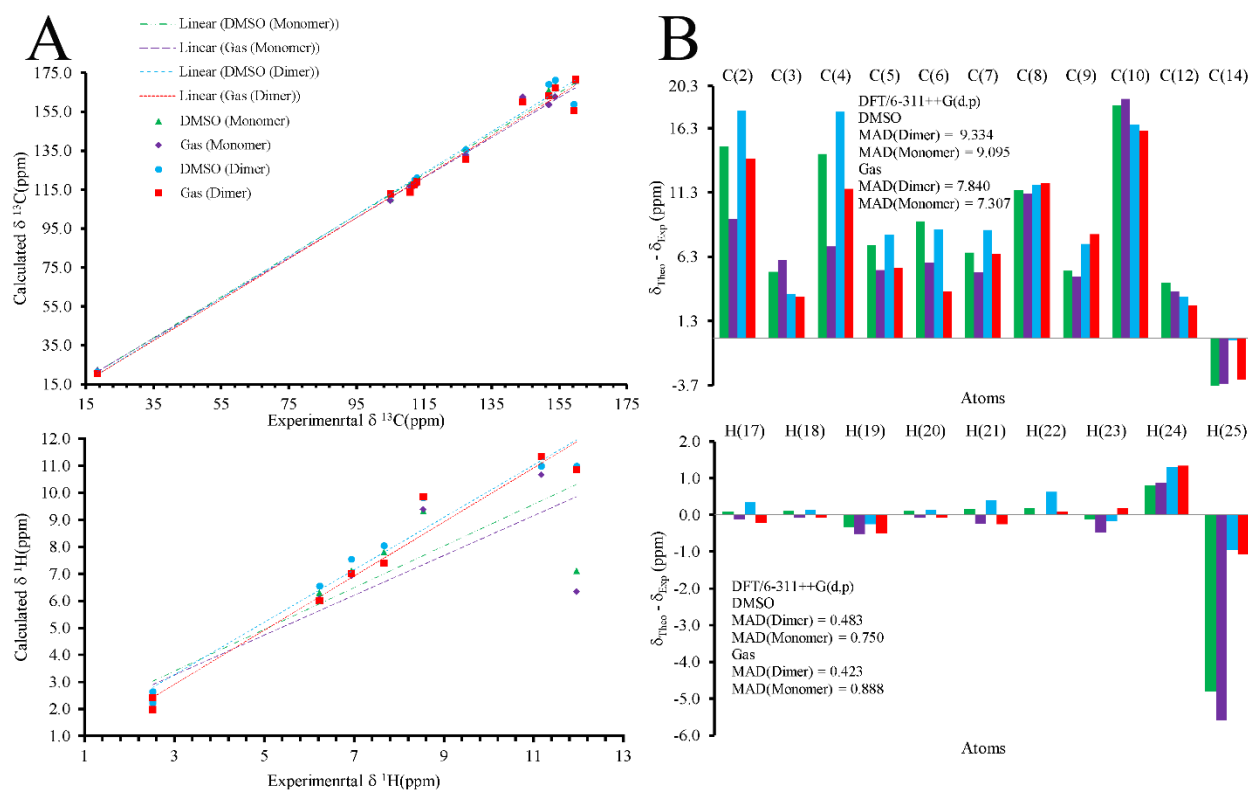


**Fig. 8.** (A) Correlation graphics of the experimental and calculated  $^1\text{H}$  and  $^{13}\text{C}$  NMR chemical shifts; (B) Deviation of the calculated  $^1\text{H}$  and  $^{13}\text{C}$  NMR chemical shifts (calculated by B3LYP methods with 6-311++G(d,p) basis set) from the experimental ones for the monomer and dimer form in vacuum and DMSO

### 3.5. NBO analysis

Natural bond orbital analysis is a very powerful tool for evaluating the molecule stability parameters including: intramolecular and intermolecular charge transfer (ICT) and delocalization of electron density (ED). Investigation of intra- and intermolecular bonds and interactions among bonds provide valuable reasons for studying the conjugative and hyperconjugative interactions. Some information about electron donor orbitals, electron acceptor orbitals and the interacting stabilization energy resulting from the second-order micro disturbance theory has been reported previously [67, 68].

The second order Fock matrix was performed to evaluate the donor–acceptor interactions in the NBO analysis [68, 69]. These interactions resulted in the loss of occupancy from the localized NBO of the idealized Lewis structure to an empty non-Lewis orbital. For each donor ( $i$ ) and acceptor ( $j$ ) orbital, the stabilization energy  $E^{(2)}$  associated with the delocalization of  $i \rightarrow j$  can be estimated by using Eq. (4).

$$E^{(2)} = \Delta E_{ij} = q_i \frac{F(i, j)^2}{\varepsilon_i \varepsilon_j}$$

, Eq. (4)

Where  $q_i$  denotes the donor orbital occupancy,  $\varepsilon_i$  and  $\varepsilon_j$  are diagonal elements and  $F(i, j)$  is the off diagonal NBO Fock matrix element.

Delocalization of electron density between occupied Lewis-type (bond or lone pair) NBO orbitals and formally unoccupied (antibond or Rydberg) non-Lewis NBO orbitals lead to a stabilizing donor–acceptor interaction. The comparison between "filled" (donors) Lewis-type NBOs and "empty" (acceptors) non-Lewis NBOs according to second-order perturbation energy values ( $E^{(2)}$  of 7-oxime) has been detailed in Table 5. In this table, only the stabilization energies of donor-acceptor interactions that were more than 4 kcal mol<sup>-1</sup> have been represented.

Also, the delocalization of ED between the occupied Lewis-type and unoccupied non-Lewis NBOs leads to stabilizing donor-acceptor interactions that have a key role in the stabilization of the entire molecular system. B3LYP/6-311++G(d,p) level (in the vacuum) can be used for estimating the strength of these interactions using the second order perturbation theory. The large  $E^{(2)}$  value in the NBO analysis confirmed the intensive interaction between electron-donors and electron-acceptors and the greater extent of conjugation in the whole system.

The intermolecular hyperconjugative interactions are caused by overlapping the bonding orbitals of (C-C), (C-N), (C-O), (C-H) and (O-H) and antibonding orbitals of (C-C), (C-N), (C-O) and (N-O). These interactions result in Intramolecular Charge Transfer (ICT) which leads to the stabilization of the whole molecular system. These interactions caused an increase in electron density (ED) of some of the antibonding orbitals and consequently, weakened the respective bonds. In 7-Oxime, the electron density of the two conjugated single as well as the double bond clearly showed strong delocalization (~1.9 e).

The strong intramolecular conjugative interaction between the  $\pi$  electrons of C=C (of the aromatic system) and the antibonding orbitals of C=C (of the ring), C=O (of the carbonyl group) and C=N (of the oxime group) led to the stabilization of some parts of the ring (**Table 5**).

Also, the intramolecular conjugative interaction resulted from the  $\pi$  electrons of the C<sub>2</sub>-O<sub>11</sub> and C<sub>14</sub>-N<sub>15</sub> (in the oxime group) to the antibonding orbitals of C<sub>3</sub>-C<sub>4</sub> and C<sub>8</sub>-C<sub>9</sub> (in the aromatic

system) caused the stabilization energy to be equal with 5.10 and 6.45 kcal mol<sup>-1</sup>, respectively. Besides, the stabilization energies of (9.08 and 24.62), (13.97, 21.5 and 18.06), (23.1 and 13.41) and (2081, 13.19 and 26.81) kcal mol<sup>-1</sup> were obtained as a result of the strong intramolecular conjugative interactions of  $\pi$  (C<sub>3</sub>-C<sub>4</sub>)  $\rightarrow$   $\pi^*$  (C<sub>5</sub>-C<sub>10</sub> and C<sub>2</sub>-O<sub>11</sub>),  $\pi$  (C<sub>5</sub>-C<sub>10</sub>)  $\rightarrow$   $\pi^*$  (C<sub>8</sub>-C<sub>9</sub>, C<sub>6</sub>-C<sub>7</sub> and C<sub>3</sub>-C<sub>4</sub>),  $\pi$  (C<sub>6</sub>-C<sub>7</sub>)  $\rightarrow$   $\pi^*$  (C<sub>8</sub>-C<sub>9</sub> and C<sub>5</sub>-C<sub>10</sub>) and  $\pi$  (C<sub>8</sub>-C<sub>9</sub>)  $\rightarrow$   $\pi^*$  (C<sub>14</sub>-N<sub>15</sub>, C<sub>6</sub>-C<sub>7</sub> and C<sub>5</sub>-C<sub>10</sub>) in the aromatic system, respectively (See Table 5).

In our molecule, the hyperconjugative interactions of  $\sigma \rightarrow \sigma^*$  transitions were also seen in the various bonds. Among these interactions,  $\sigma$  (C<sub>3</sub>-H<sub>17</sub>)  $\rightarrow$   $\sigma^*$  (C<sub>4</sub>-C<sub>5</sub>) and  $\sigma$  (C<sub>9</sub>-C<sub>14</sub>)  $\rightarrow$   $\sigma^*$  (N<sub>15</sub>-O<sub>16</sub>) showed the biggest energetic contribution of their interactions at 5.15 and 4.82 kcal mol<sup>-1</sup>, respectively.

The other important intramolecular charge transfers have been detailed in Table 5. Furthermore, both the hyperconjugative interactions of the  $\sigma \rightarrow \pi^*$  transitions from C<sub>12</sub>-H<sub>18</sub> and C<sub>12</sub>-H<sub>20</sub> bonds (in the methyl group) to the antibonding orbitals of C<sub>3</sub>-C<sub>4</sub> (in vinyl group of the pyrone ring) led to the stabilization energy of 4.09 kcal mol<sup>-1</sup>.

In addition, the other important interaction energies resulted from  $n \rightarrow \sigma^*$  transitions, defined as intramolecular resonance, were donating electrons from the LP(1) O<sub>1</sub> and LP(2) O<sub>11</sub> atoms (of the electron donating group in the lactone group of the pyrone ring) to the anti-bonding acceptors ( $\sigma^*$ ) of C<sub>5</sub>-C<sub>10</sub>, C<sub>2</sub>-C<sub>3</sub>, C<sub>2</sub>-C<sub>3</sub> and O<sub>1</sub>-C<sub>2</sub> with stabilization energies of 6.14, 4.1, 15.61 and 40.25 kcal mol<sup>-1</sup>. Also, the charge transferred from LP(1) O<sub>13</sub> atom of the hydroxyl group to the  $\sigma^*$  (C<sub>8</sub>-C<sub>9</sub>) created the stabilization energy of about 6.74 kcal mol<sup>-1</sup>.

**Table 5.** Second order perturbation theory analysis of Fock matrix of the title compound calculated by NBO method (by using B3LYP/6-311++G(d,p) level)

Donor (i)	Type	ED/e <sup>a</sup>	Acceptor (j)	Type	ED/e <sup>a</sup>	E <sup>(2)</sup> <sup>b</sup> (kcal mol <sup>-1</sup> )	E <sub>j</sub> - E <sub>i</sub> <sup>c</sup> (a.u.)	F(i,j) <sup>d</sup> (a.u.)
C <sub>2</sub> -C <sub>3</sub>	σ	1.98132	C <sub>4</sub> -C <sub>12</sub>	σ*	0.01708	4.3	1.1	0.061
C <sub>2</sub> -O <sub>11</sub>	π	1.98076	C <sub>3</sub> -C <sub>4</sub>	π*	0.18321	5.1	0.41	0.042
C <sub>3</sub> -C <sub>4</sub>	π	1.80837	C <sub>5</sub> -C <sub>10</sub>	π*	0.42205	9.08	0.29	0.049
C <sub>3</sub> -C <sub>4</sub>	π	1.80837	C <sub>2</sub> -O <sub>11</sub>	π*	0.28726	24.62	0.3	0.078
C <sub>3</sub> -H <sub>17</sub>	σ	1.97469	C <sub>4</sub> -C <sub>5</sub>	σ*	0.03095	5.15	1.01	0.064
C <sub>3</sub> -H <sub>17</sub>	σ	1.97469	O <sub>1</sub> -C <sub>2</sub>	σ*	0.1334	4.7	0.81	0.057
C <sub>5</sub> -C <sub>6</sub>	σ	1.95713	O <sub>1</sub> -C <sub>10</sub>	σ*	0.031	4.69	1.04	0.063
C <sub>5</sub> -C <sub>10</sub>	σ	1.96032	C <sub>9</sub> -C <sub>10</sub>	σ*	0.02561	4.21	1.23	0.064
C <sub>5</sub> -C <sub>10</sub>	π	1.60337	C <sub>8</sub> -C <sub>9</sub>	π*	0.4373	13.97	0.28	0.056
C <sub>5</sub> -C <sub>10</sub>	π	1.60337	C <sub>6</sub> -C <sub>7</sub>	π*	0.29638	21.5	0.29	0.072
C <sub>5</sub> -C <sub>10</sub>	π	1.60337	C <sub>3</sub> -C <sub>4</sub>	π*	0.18321	18.06	0.3	0.069
C <sub>6</sub> -C <sub>7</sub>	π	1.73079	C <sub>8</sub> -C <sub>9</sub>	π*	0.4373	23.1	0.28	0.074
C <sub>6</sub> -C <sub>7</sub>	π	1.73079	C <sub>5</sub> -C <sub>10</sub>	π*	0.42205	13.41	0.28	0.057
C <sub>7</sub> -H <sub>22</sub>	σ	1.97799	C <sub>5</sub> -C <sub>6</sub>	σ*	0.02112	4.05	1.06	0.058
C <sub>8</sub> -C <sub>9</sub>	π	1.60915	C <sub>14</sub> -N <sub>15</sub>	π*	0.19054	20.81	0.26	0.07
C <sub>8</sub> -C <sub>9</sub>	π	1.60915	C <sub>6</sub> -C <sub>7</sub>	π*	0.29638	13.19	0.29	0.057
C <sub>8</sub> -C <sub>9</sub>	π	1.60915	C <sub>5</sub> -C <sub>10</sub>	π*	0.42205	26.9	0.28	0.078
C <sub>9</sub> -C <sub>10</sub>	σ	1.9686	C <sub>5</sub> -C <sub>10</sub>	σ*	0.03038	4.49	1.25	0.067
C <sub>9</sub> -C <sub>14</sub>	σ	1.96668	N <sub>15</sub> -O <sub>16</sub>	σ*	0.02693	4.82	0.91	0.059
C <sub>12</sub> -H <sub>18</sub>	σ	1.97449	C <sub>3</sub> -C <sub>4</sub>	π*	0.18321	4.09	0.54	0.044
C <sub>12</sub> -H <sub>19</sub>	σ	1.98877	C <sub>4</sub> -C <sub>5</sub>	σ*	0.03095	4.44	1	0.06
C <sub>12</sub> -H <sub>20</sub>	σ	1.97449	C <sub>3</sub> -C <sub>4</sub>	π*	0.18321	4.09	0.54	0.044
C <sub>14</sub> -N <sub>15</sub>	π	1.9561	C <sub>8</sub> -C <sub>9</sub>	π*	0.4373	6.45	0.36	0.048
N <sub>15</sub>	n <sub>1</sub>	1.91798	C <sub>14</sub> -H <sub>24</sub>	σ*	0.02425	6.45	0.86	0.068
N <sub>15</sub>	n <sub>1</sub>	1.91798	O <sub>13</sub> -H <sub>23</sub>	σ*	0.05723	18.92	0.86	0.115
O <sub>1</sub>	n <sub>2</sub>	1.7474	C <sub>5</sub> -C <sub>10</sub>	π*	0.42205	31.25	0.35	0.098
O <sub>1</sub>	n <sub>1</sub>	1.96141	C <sub>5</sub> -C <sub>10</sub>	σ*	0.03038	6.14	1.08	0.073
O <sub>1</sub>	n <sub>2</sub>	1.7474	C <sub>2</sub> -O <sub>11</sub>	π*	0.28726	31.93	0.36	0.096
O <sub>1</sub>	n <sub>1</sub>	1.96141	C <sub>2</sub> -C <sub>3</sub>	σ*	0.05294	4.1	1.01	0.058
O <sub>11</sub>	n <sub>2</sub>	1.82692	C <sub>2</sub> -C <sub>3</sub>	σ*	0.05294	15.61	0.72	0.097
O <sub>11</sub>	n <sub>2</sub>	1.82692	O <sub>1</sub> -C <sub>2</sub>	σ*	0.1334	40.25	0.54	0.133
O <sub>13</sub>	n <sub>2</sub>	1.81292	C <sub>8</sub> -C <sub>9</sub>	π*	0.4373	37.38	0.33	0.106
O <sub>13</sub>	n <sub>1</sub>	1.97363	C <sub>8</sub> -C <sub>9</sub>	σ*	0.0327	6.74	1.11	0.077
O <sub>13</sub> -H <sub>23</sub>	σ	1.98391	C <sub>7</sub> -C <sub>8</sub>	σ*	0.02339	4.68	1.29	0.07
O <sub>16</sub>	n <sub>2</sub>	1.90842	C <sub>14</sub> -N <sub>15</sub>	π*	0.19054	16.47	0.33	0.068

<sup>a</sup> Electron density, <sup>b</sup> Energy of hyper conjugative interaction (stabilization energy), <sup>c</sup> Energy difference between donor and acceptor i and j NBO orbitals, <sup>d</sup> The Fock matrix element between i and j NBO orbitals.

The NBO analysis is an effective tool for the chemical interpretation of hyperconjugative interactions and electron density transfer (EDT) from filled lone electron pairs of the n(Y) of the “Lewis-base” Y to the unfilled anti-bond  $\sigma$  (X-H) of the “Lewis-acid” X-H in X-H...Y hydrogen bonding system [70]. In our molecule, a strong interaction observed between the lone pair of N<sub>15</sub> (LP(1)) and the anti-bonding acceptor of the hydroxyl group ( $\sigma^*$  (O<sub>13</sub>-H<sub>23</sub>)) with the stabilization energy of 18.92 kcal mol<sup>-1</sup>, confirming the presence of an intramolecular interaction between the hydrogen atom in the hydroxyl group (H<sub>23</sub>) and the nitrogen atom in the oxime group (N<sub>15</sub>).

Comparing the NBO analysis results of the monomer with that of the dimer clearly showed the existence of strong intermolecular hydrogen bonds between two monomers and the formation of the dimer form. This investigation obviously identified the formation of four strong intermolecular H-bonded interactions in the dimer form: LP(1) (O<sub>11</sub>)  $\rightarrow$   $\sigma^*$  (O<sub>41</sub>-H<sub>50</sub>), LP(2) (O<sub>11</sub>)  $\rightarrow$   $\sigma^*$  (O<sub>41</sub>-H<sub>50</sub>), LP(1) (O<sub>36</sub>)  $\rightarrow$   $\sigma^*$  (O<sub>16</sub>-H<sub>25</sub>) and LP(2) O<sub>36</sub>  $\rightarrow$   $\sigma^*$  (O<sub>16</sub>-H<sub>25</sub>) with the stabilization energies of 3.27, 8.04, 3.27 and 8.04 kcal mol<sup>-1</sup>, respectively (Table 6).

**Table 6.** Second order perturbation theory analysis of Fock matrix for the dimer form of the title compound calculated by NBO method (by using B3LYP/6-311++G(d,p) level)

Donor (i)	Type	ED/e <sup>a</sup>	Acceptor (j)	Type	ED/e	E <sup>(2)</sup> <sup>b</sup> (kcal mol <sup>-1</sup> )	E <sub>j</sub> - E <sub>i</sub> <sup>c</sup> (a.u.)	F(i,j) <sup>d</sup> (a.u.)
From unit 1 to unit 2								
C <sub>2</sub> -C <sub>3</sub>	σ	1.98041	O <sub>41</sub> -H <sub>50</sub>	σ*	0.03264	0.24	1.14	0.015
C <sub>2</sub> -O <sub>11</sub>	π	1.98272	O <sub>41</sub> -H <sub>50</sub>	σ*	0.03264	0.15	0.82	0.01
C <sub>14</sub> -N <sub>15</sub>	π	1.94808	C <sub>39</sub> -N <sub>40</sub>	π*	0.18709	0.05	0.35	0.004
C <sub>14</sub> -H <sub>24</sub>	σ	1.98133	C <sub>39</sub> -H <sub>49</sub>	σ*	0.02877	0.1	0.95	0.009
N <sub>15</sub> -O <sub>16</sub>	σ	1.98728	O <sub>26</sub>	n <sub>1</sub>	0.00605	0.09	1.57	0.011
O <sub>16</sub> -H <sub>25</sub>	σ	1.98833	O <sub>26</sub>	n <sub>1</sub>	0.00605	0.07	1.46	0.009
O <sub>16</sub> -H <sub>25</sub>	σ	1.98833	C <sub>27</sub> -O <sub>36</sub>	σ*	0.01489	0.08	1.33	0.009
O <sub>11</sub>	n <sub>1</sub>	1.97104	O <sub>41</sub> -H <sub>50</sub>	σ*	0.03264	3.27	1.13	0.054
O <sub>11</sub>	n <sub>2</sub>	1.83875	O <sub>41</sub>	n <sub>4</sub>	0.00021	0.08	1.46	0.01
O <sub>11</sub>	n <sub>2</sub>	1.83875	O <sub>41</sub>	n <sub>6</sub>	0.00006	0.09	1.38	0.01
O <sub>11</sub>	n <sub>2</sub>	1.83875	H <sub>50</sub>	n <sub>1</sub>	0.00259	0.19	1.65	0.017
O <sub>11</sub>	n <sub>2</sub>	1.83875	H <sub>50</sub>	n <sub>6</sub>	0.00006	0.06	2.55	0.012
<b>O<sub>11</sub></b>	<b>n<sub>2</sub></b>	<b>1.83875</b>	<b>O<sub>41</sub>-H<sub>50</sub></b>	<b>σ*</b>	<b>0.03264</b>	<b>8.04</b>	<b>0.7</b>	<b>0.069</b>
N <sub>15</sub>	n <sub>1</sub>	1.91303	C <sub>39</sub>	n <sub>11</sub>	0.0001	0.09	1.44	0.011
O <sub>16</sub>	n <sub>1</sub>	1.98778	C <sub>27</sub> -O <sub>36</sub>	σ*	0.01489	0.09	1.23	0.009
<b>O<sub>16</sub></b>	<b>n<sub>1</sub></b>	<b>1.98778</b>	<b>C<sub>39</sub>-H<sub>49</sub></b>	<b>σ*</b>	<b>0.02877</b>	<b>0.37</b>	<b>1.05</b>	<b>0.018</b>
O <sub>16</sub>	n <sub>2</sub>	1.89086	C <sub>27</sub>	n <sub>1</sub>	0.01368	0.06	1.44	0.009
<b>O<sub>16</sub></b>	<b>n<sub>2</sub></b>	<b>1.89086</b>	<b>C<sub>39</sub>-H<sub>49</sub></b>	<b>σ*</b>	<b>0.02877</b>	<b>0.26</b>	<b>0.74</b>	<b>0.013</b>
From unit 2 to unit 1								
C <sub>27</sub> -C <sub>28</sub>	σ	1.98041	O <sub>16</sub> -H <sub>25</sub>	σ*	0.03264	0.24	1.14	0.015
C <sub>27</sub> -O <sub>36</sub>	π	1.98272	O <sub>16</sub> -H <sub>25</sub>	σ*	0.03264	0.15	0.82	0.01
C <sub>39</sub> -N <sub>40</sub>	π	1.94808	C <sub>14</sub> -N <sub>15</sub>	π*	0.18709	0.05	0.35	0.004
C <sub>39</sub> -H <sub>49</sub>	σ	1.98133	C <sub>14</sub> -H <sub>24</sub>	σ*	0.02877	0.1	0.95	0.009
N <sub>40</sub> -O <sub>41</sub>	σ	1.98728	O <sub>1</sub>	n <sub>1</sub>	0.00605	0.09	1.57	0.011
O <sub>41</sub> -H <sub>50</sub>	σ	1.98833	O <sub>1</sub>	n <sub>1</sub>	0.00605	0.07	1.46	0.009
O <sub>41</sub> -H <sub>50</sub>	σ	1.98833	C <sub>2</sub> -O <sub>11</sub>	σ*	0.01489	0.08	1.33	0.009
<b>O<sub>36</sub></b>	<b>n<sub>1</sub></b>	<b>1.97104</b>	<b>O<sub>16</sub>-H<sub>25</sub></b>	<b>σ*</b>	<b>0.03264</b>	<b>3.27</b>	<b>1.13</b>	<b>0.054</b>
O <sub>36</sub>	n <sub>2</sub>	1.83875	O <sub>16</sub>	n <sub>4</sub>	0.00021	0.08	1.46	0.01
O <sub>36</sub>	n <sub>2</sub>	1.83875	O <sub>16</sub>	n <sub>6</sub>	0.00006	0.09	1.38	0.01
O <sub>36</sub>	n <sub>2</sub>	1.83875	H <sub>25</sub>	n <sub>1</sub>	0.00259	0.19	1.65	0.017
O <sub>36</sub>	n <sub>2</sub>	1.83875	H <sub>25</sub>	n <sub>6</sub>	0.00006	0.06	2.55	0.012
<b>O<sub>36</sub></b>	<b>n<sub>2</sub></b>	<b>1.83875</b>	<b>O<sub>16</sub>-H<sub>25</sub></b>	<b>σ*</b>	<b>0.03264</b>	<b>8.04</b>	<b>0.7</b>	<b>0.069</b>
N <sub>40</sub>	n <sub>1</sub>	1.91302	C <sub>14</sub>	n <sub>11</sub>	0.0001	0.09	1.44	0.011
O <sub>41</sub>	n <sub>1</sub>	1.98778	C <sub>2</sub> -O <sub>11</sub>	σ*	0.01489	0.09	1.23	0.009
<b>O<sub>41</sub></b>	<b>n<sub>1</sub></b>	<b>1.98778</b>	<b>C<sub>14</sub>-H<sub>24</sub></b>	<b>σ*</b>	<b>0.02877</b>	<b>0.37</b>	<b>1.05</b>	<b>0.018</b>
O <sub>41</sub>	n <sub>2</sub>	1.89085	C <sub>2</sub>	n <sub>1</sub>	0.01368	0.06	1.44	0.009
<b>O<sub>41</sub></b>	<b>n<sub>2</sub></b>	<b>1.89085</b>	<b>C<sub>14</sub>-H<sub>24</sub></b>	<b>σ*</b>	<b>0.02877</b>	<b>0.27</b>	<b>0.74</b>	<b>0.013</b>

<sup>a</sup> ED-Electron density, <sup>b</sup> E(2) means energy of hyper conjugative interaction (stabilization energy), <sup>c</sup> Energy difference between donor and acceptor i and j NBO orbitals, <sup>d</sup> F(i,j) is the Fock matrix element between i and j NBO orbitals.

### 3.6. MEP

The calculated MEP parameter of the title compound has been depicted in Fig. 9. The molecular electrostatic potential  $V(r)$ , at a given point  $r(x, y, z)$  in the vicinity of a molecule, is defined as the energy of interaction between the electrical charge produced by the molecule electrons and nuclei and the positive test charge (of a proton) located at  $r$  [71]. The negative (red) regions of MEP display the electrophilic sites while the positive (blue) ones show the nucleophilic sites. As illustrated in Fig. 9, the negative region was mainly localized on the oxygen atoms (O<sub>11</sub>, O<sub>1</sub>, O<sub>16</sub> and O<sub>13</sub>), whereas the nucleophilic reactivity of the molecule was mainly existed on the proton of the oxime group.

The MEP map of 7-Oxime suggests that the calculated electrostatic potential fluctuated between the oxygen atoms of the lactone group (dark yellow), the hydrogen atoms of the oxime group (dark blue) and the aromatic ring system (green). From MEP map, the oxygen atoms were the most electronegative positions and have enormous negative charge while the hydrogen atoms attached to the oxime group possessed the positive charge (blue region). The order colors were red < orange < yellow < green < blue and the color code of these maps was in the range between -1.0 (darkest red) and +1.0 (darkest blue) in all compounds.

The blue color indicates the strongest attraction while the red color indicates the strongest repulsion. Also, the maximum negative potential values (dark yellow) were located on the oxygen atoms of the lactone group (-0.0579) while the maximum positive region (dark blue) were localized on the H<sub>25</sub> atom of the oxime group (+0.06422). These data also confirmed the presence of an intermolecular interaction between two monomers and the formation of the dimer form.

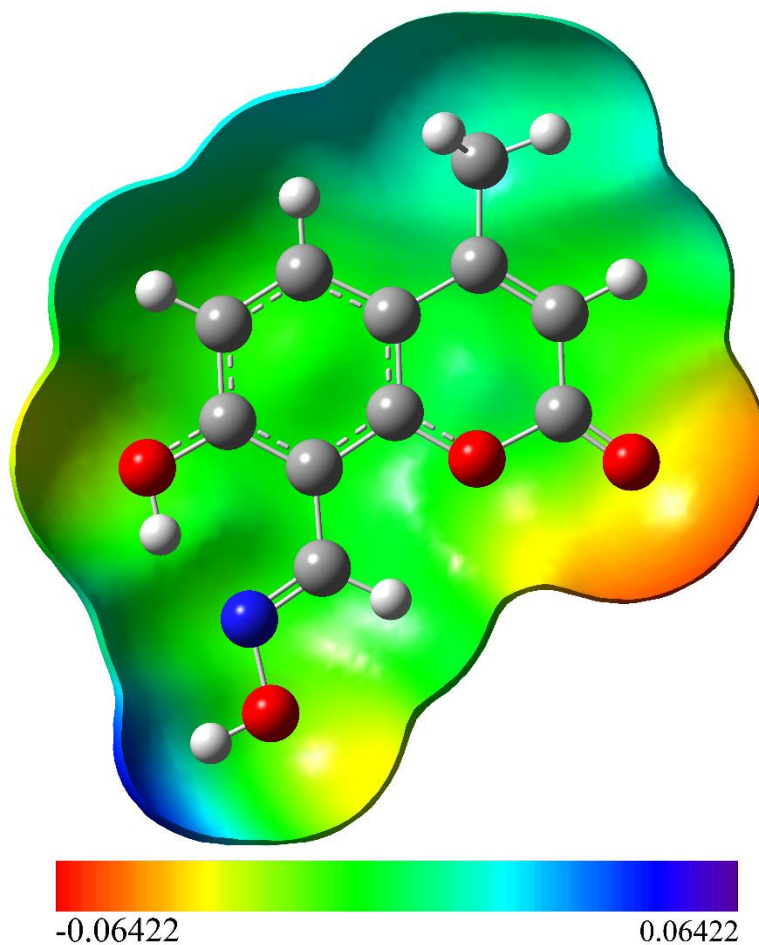


**Fig. 9.** The molecular electrostatic potential (MEP) map for 7-oxime (calculated at B3LYP/6-311++G(d,p) level)

### 3.7. Thermodynamic Properties

Partition functions, as an important parameter in thermodynamics, can be used to calculate heat capacities, entropies, equilibrium constants and rate constants obtained from the theoretical harmonic frequencies [72]. Herein, the statistical thermochemical analysis of the title compound was performed by considering the existence of 7-Oxime at 298.15 K and one atmospheric pressure. The thermodynamic parameters of the monomer and dimer forms; such as zero-point vibrational energy, thermal energy, specific heat capacity, rotational constants, dipole moment and entropy were calculated using DFT/B3LYP method and 6-311++G(d,p) basis set and the results have been detailed in Table 7.

**Table 7.** The calculated thermodynamical parameters of the title compound in ground state at 298.15 K and one atmospheric pressure for the monomer and dimer forms.

Basic set	B3LYP/6-311++G(d,p)	
	Monomer	Dimer
SCF energy $E$ (a.u)	-780.239	-1560.868
Zero point vibrational energy (kcal mol <sup>-1</sup> )	115.897	233.713
<i>Rotational constants (GHz)</i>		
A	0.826	0.206
B	0.401	0.0854
C	0.270	0.071
Thermal energy (kcal mol <sup>-1</sup> )	124.462	251.347
Heat capacity $C_v$ (Cal mol <sup>-1</sup> K <sup>-1</sup> )	52.936	108.679
Entropy $S$ (cal mol <sup>-1</sup> K <sup>-1</sup> )	114.873	185.719
Dipole moment $I$ (Debye)	4.361	6.200

As depicted in Table 8, the computed thermodynamic parameters increased by increasing the temperature from 100 to 700 K. The possible reason for this issue is the fact that the increased temperature can change the molecular vibrational intensities [72]. In addition, the correlation equations between heat capacity, entropy, enthalpy changes with temperature were fitted by quadratic formula. The corresponding fitting factors ( $R^2$ ) were obtained to be 0.99989, 0.99998 and 0.99982 for these thermodynamic properties, respectively. Eqs. (5-7) and Fig. 10 depicts the corresponding fitting equations of the title compound in the vacuum and their correlation graphics obtained by DFT/B3LYP method with 6-311++G(d,p) basis set.

$$C_{p,m}^0 = 0.661 + 0.205T - 1 \times 10^{-4} T^2 (R^2 = 0.99989) , \text{ Eq. (5)}$$

$$S_m^0 = 54.01 + 0.221T - 6 \times 10^{-5} T^2 (R^2 = 0.99998) , \text{ Eq. (6)}$$

$$H_m^0 = -1.091 + 0.015T + 6 \times 10^{-5} T^2 (R^2 = 0.99982) , \text{ Eq. (7)}$$

All of these thermodynamic data provided helpful information for further studies on our molecule. It should be mentioned that all of the thermodynamic calculations were done in the vacuum and they could not be used in the solution.

**Table 8.** Thermodynamic properties of the title compound at different temperatures at the B3LYP/6-311++G(d,p) level in the vacuum

T (k)	$C_{p,m}$ (Cal mol <sup>-1</sup> k <sup>-1</sup> )	$S_m^\circ$ (Cal mol <sup>-1</sup> k <sup>-1</sup> )	$\Delta H_m^\circ$ (Cal mol <sup>-1</sup> k <sup>-1</sup> )
100	20.678	75.259	1.399
150	29.236	86.080	2.748
200	37.480	96.197	4.516
250	45.492	105.869	6.691
298.15	52.936	114.873	9.157
300	53.215	115.214	9.259
350	60.526	124.278	12.204
400	67.308	133.075	15.502
450	73.496	141.600	19.124
500	79.078	149.847	23.040
550	84.086	157.813	27.221
600	88.569	165.498	31.638
650	92.587	172.908	36.269
700	96.198	180.051	41.089

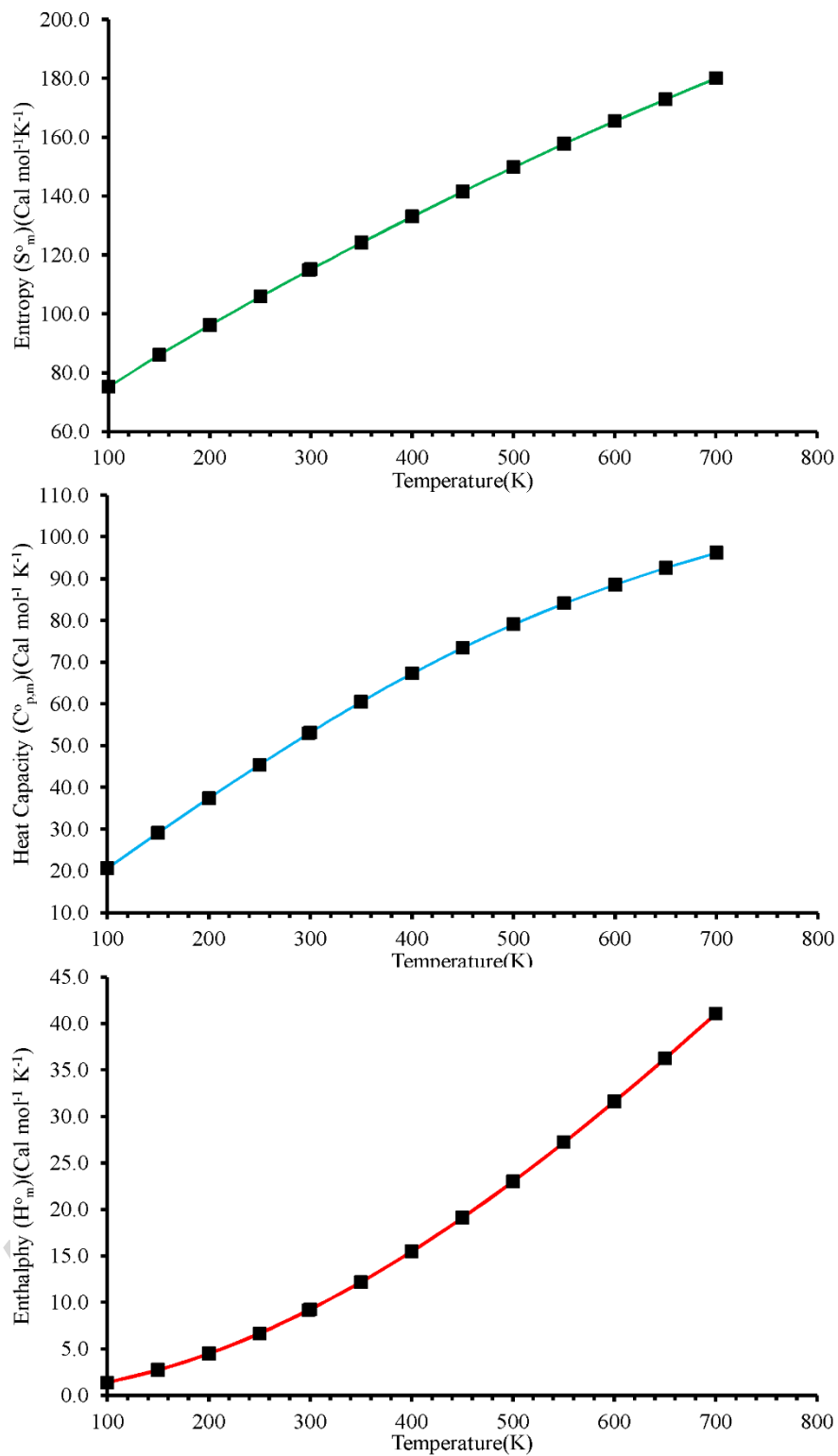


**Fig. 10.** Correlation graphic of entropy, heat capacity, enthalpy with temperature for the title compound

### 3.8. Molecular docking results

Today, diabetes mellitus (DM) is one of the major problems throughout the world which has caused global concerns for people and medical departments. Basically, DM is classified in two groups including type 1 DM (T1DM) and type 2 DM (T2DM)[73]. Generally, T1DM is considered as insulin-dependent diabetes and is an autoimmune condition [74]. Type 2 DM; formerly known as non-insulin dependent diabetes; is the most common type of DM identified by hyperglycemia, insulin deficiency and insulin resistance [9, 75]. After degradation of food materials (*e.g.* starch), sugar digestive enzymes (*i.e.*  $\alpha$ -amylase and  $\alpha$ -glucosidase) break down complex carbohydrates into smaller units. Then, these simple units (*i.e.* glucose molecules) will absorb across intestinal tissues [76, 77].

The absorbed glucose will move to the liver by the portal venous system. After its entrance into blood circulation, the pancreas islets will release insulin to support glucose to transport from blood into the cells [78] (Fig. 11). Patients with T2DM have highest amount of glucose molecules in their body and their body cells are not sufficiently sensitive to enter glucose molecules [79]. Therefore, this simple sugar accumulates in their body and can cause hyperglycemia [80]. From this point of view; it seems that the inhibition of carbohydrates digestive enzymes can be considered as a primary policy to decrease the incidence of T2DM.

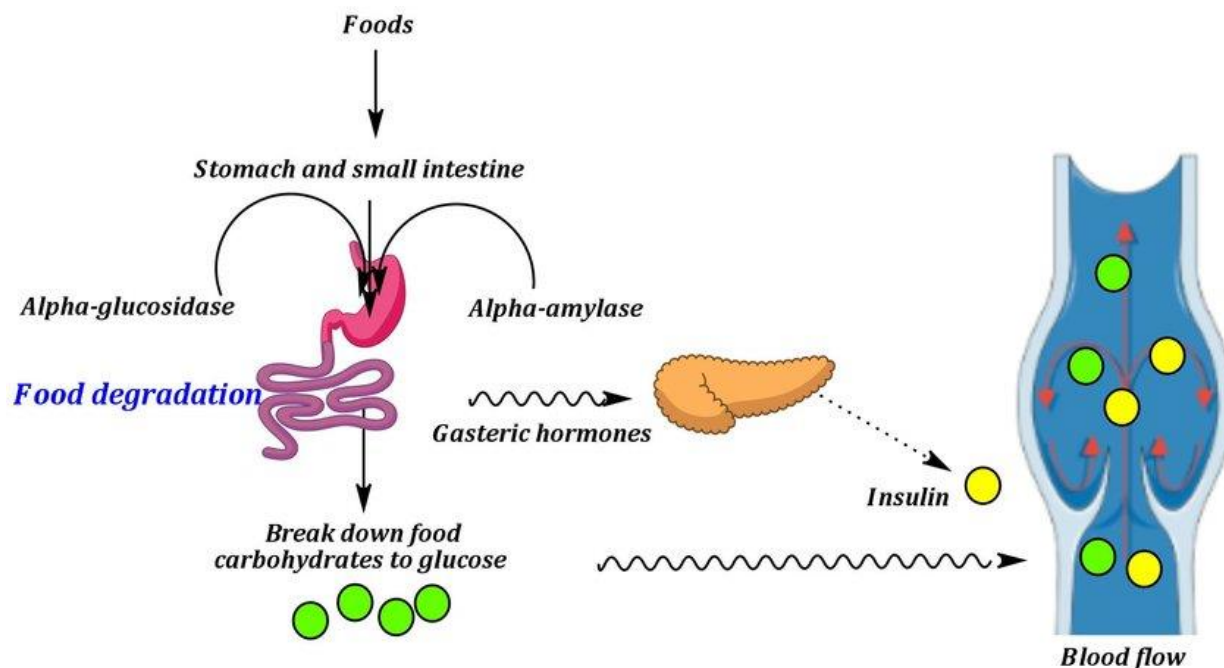


**Fig. 11.** The simple pathway for food degradation and glucose absorption in the body.

Many studies indicated that the protein encoded by genes involved in carbohydrate digestion process can affect many different proteins in human body [81]. As shown in Fig. 12, these proteins have specific signaling pathways which can affect a large number of proteins in human body. These signaling pathways suggested that the inhibition of these enzymes can regulate or modulate the activity of other upstream/downstream proteins (or genes). Therefore, the inhibition of these enzymes can ameliorate the post-effects of their signaling pathways in DM.

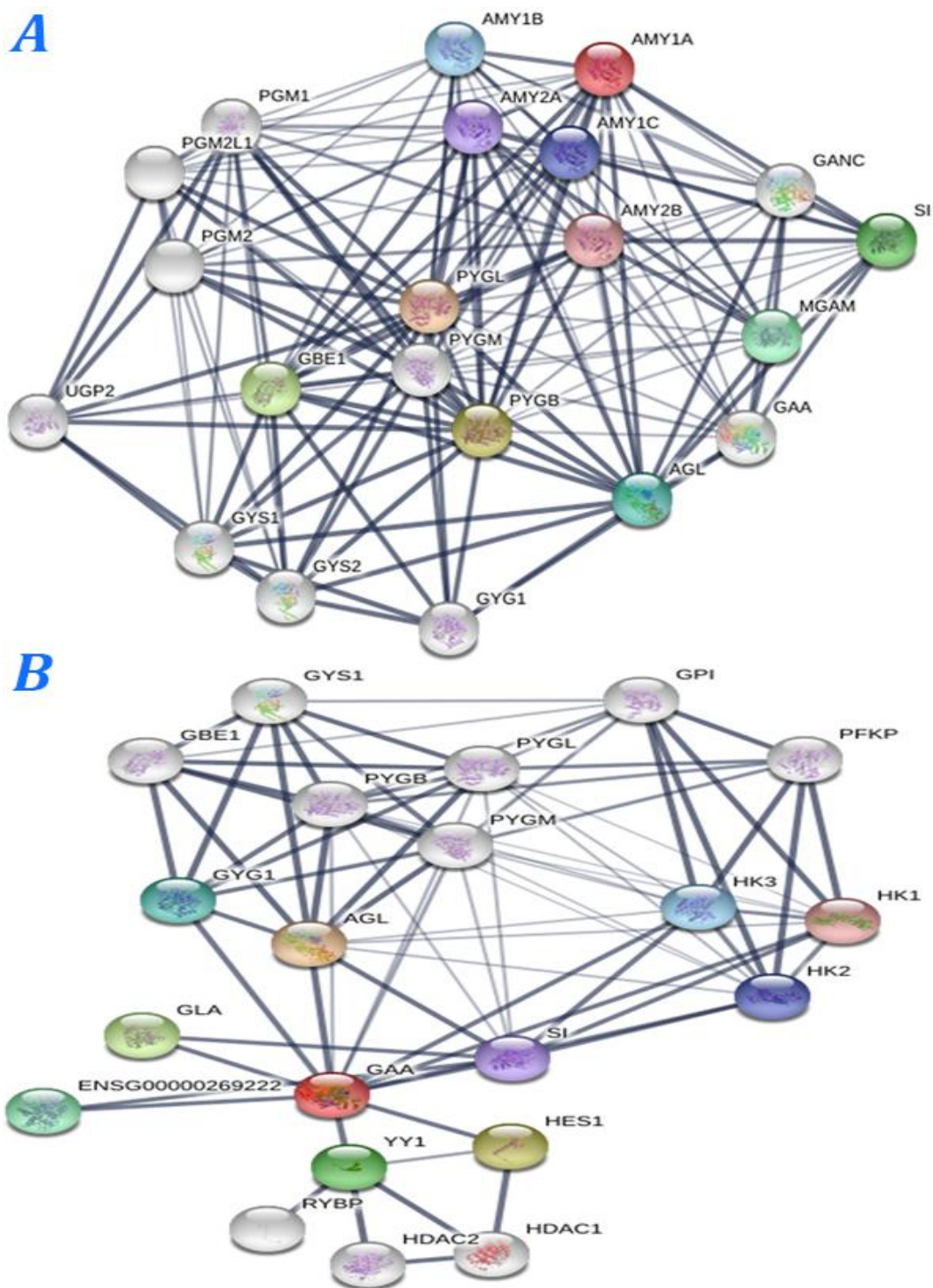


**Fig. 12.** The signaling pathways of (A)  $\alpha$ -amylase (AMY1A) and (B)  $\alpha$ -glucosidase (GAA).

On the other hand, inhibition of  $\alpha$ -glucosidase and  $\alpha$ -amylase activity can control the level of blood glucose to avoid hyperglycemia [75]. Therefore, finding the best inhibitor for these enzymes can be considered as a primary approach in the pre-management of DM.

Coumarins are known as a chemically diverse category of non-toxic secondary and reactive metabolites which are produced in plant tissues (*e.g.* seeds, roots and leaves) and exhibit a wide range of biological activities including anti-diabetic, anti-inflammatory, antioxidant and anticancer potential [82-84].

In an interesting study, Verma and coworkers [85] showed that scopoletin (coumarin derivative) has significant hypolipidemic and hypoglycemic effects in streptozotocin induced diabetic rats [85]. In another study, Ramu and Vijayakumar [86] reported that the 7-methoxycoumarin isolated from *Rhizophora mucronata* can obviously show *in vitro* and *in vivo* anti-diabetic potential. Recently, Wang and others [87] synthesized different coumarin derivatives which showed anti-diabetic potential.

However, due to the biological activity of coumarins and their derivatives, the possible anti-diabetic potential of 7-Oxime examined via molecular docking (fully blind docking) to provide useful information about its possible interaction with enzymes involved in T2DM. The results indicated that the mentioned compound strongly interacted with the studied active sites. The calculated docking energies for the interaction between 7-Oxime/ $\alpha$ -glucosidase and 7-Oxime/ $\alpha$ -amylase were -11.43 and -10.67 kcal·mol<sup>-1</sup>, respectively. As shown in Fig. 13, the title compound was located in the nearest catalytic residues in both active sites and constructed hydrogen bonds with this residues. Amino acids such as Trp<sup>59</sup>, Tyr<sup>62</sup>, Arg<sup>195</sup>, Asp<sup>197</sup>, Glu<sup>233</sup> and Asp<sup>300</sup> are critical residues in the active site of human  $\alpha$ -amylase which handle its activity [34]. Many studies suggested that  $\alpha$ -amylase inhibitors bound to these residues and therefore inhibited the activity of this enzyme [9, 88]. Herein, 7-Oxime interacted with these residues and this type of interaction can prove the possible inhibitory activity of this compound against this enzyme.

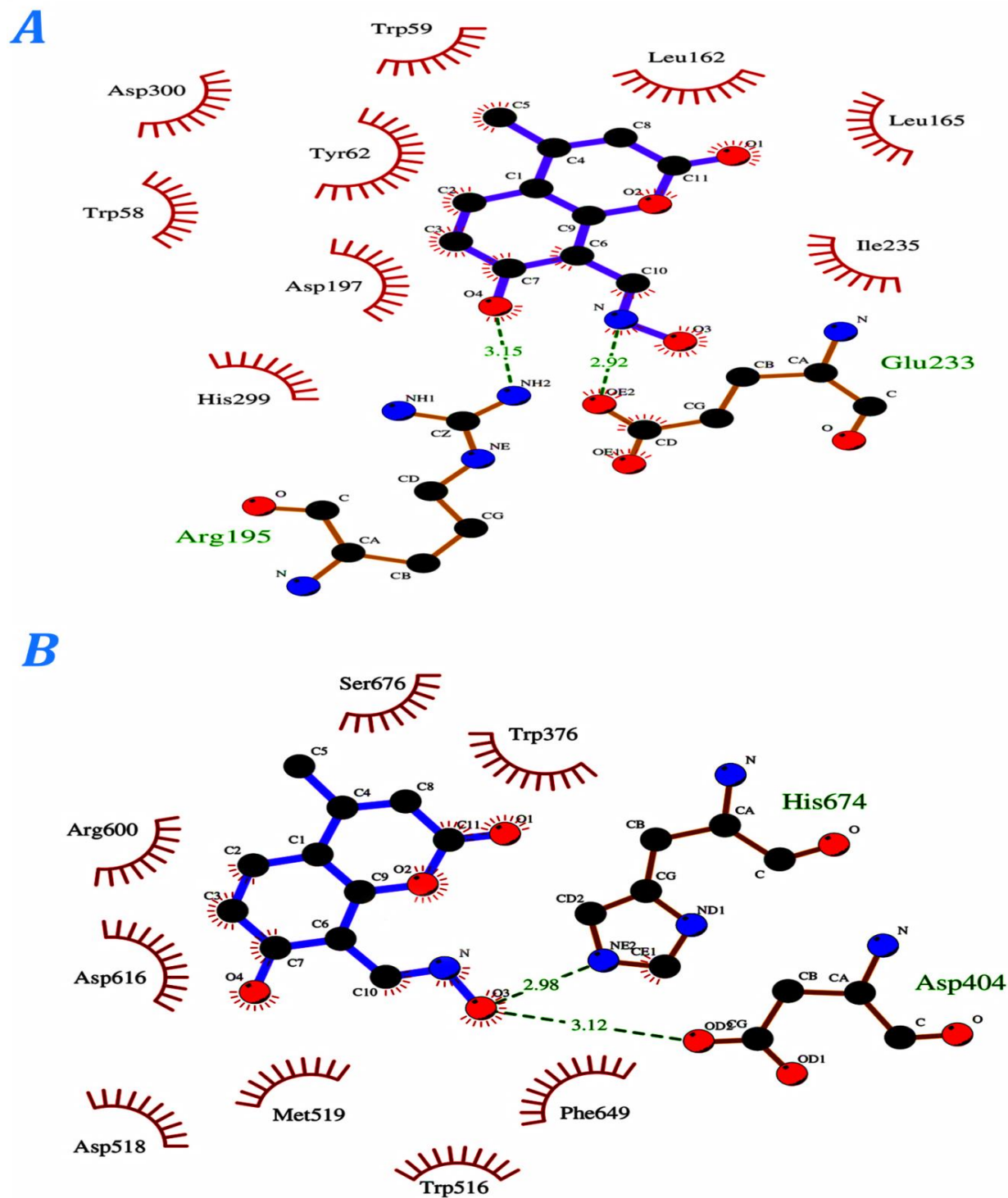


**Fig. 13.** The generated 2D plots for interaction of 7-Oxime with (A) human  $\alpha$ -amylase (1HNY) and (B) human  $\alpha$ -glucosidase (5NN8).

As shown in this Figure, the title compound constructed significant H-bonds with Glu<sup>233</sup> and Arg<sup>195</sup> in the active site of human  $\alpha$ -amylase. Our residues in this region are located in the vicinity of the docked ligand and they also participated in the observed interactions.

The  $\alpha$ -glucosidase active site has different amino acids such as Trp<sup>376</sup>, Asp<sup>404</sup>, Trp<sup>516</sup>, Asp<sup>518</sup>, Met<sup>519</sup>, Arg<sup>600</sup>, Asp<sup>616</sup>, Phe<sup>649</sup> and His<sup>674</sup> residues which are associated with its activity to digest complex carbohydrates [33]. Our compound directly bound to these residues and located in the deepest region of this active site. The title compound significantly constructed H-bonds with Asp<sup>404</sup> and His<sup>674</sup> in the active site of human  $\alpha$ -glucosidase. The docking energies showed that this compound has higher tendency to interact with the active site of  $\alpha$ -glucosidase rather than  $\alpha$ -amylase. Studies suggested that  $\alpha$ -glucosidase inhibitors can improve the health condition of patients with T2DM.

Currently, different classes of these compounds (*e.g.* acarbose, miglitol and voglibose) are available in market and widely used to treat DM [89-91]. Due to the associated adverse effects with some of these drugs [92], trying to search and find new effective compounds with low or no side effects should be considered in drug design policies. However, stopping sugar digestion and absorption provides a possible alternative way to the other methods for the management of DM. During the last decade, various papers have emphasized the influence of natural products (especially polyphenols and coumarins) on handling DM by inhibiting the carbohydrate digestive enzymes [85, 93, 94]. Therefore, considering these classes of natural products and their derivatives as supplementary agents in the management of DM may be useful for clinical therapeutics programs.

### 3.9. FMO analysis

Frontier Molecular Orbitals (FMOs) are the most important orbitals in chemical reactions. HOMO orbitals represent the ability of donating electron while LUMO orbitals represent the ability of obtaining electrons. In this work, the electronic structures of ligand/ $\alpha$ -amylase and ligand/ $\alpha$ -glucosidase complexes were isolated from the active site with the radius of 4 Å around the ligand. Moreover, the free ligand were investigated to perform further analysis in the vacuum by using B3LYP method with 6-311++G(d,p) basis set (Table 9).

According to our results, the computed values of the band gaps for ligand/ $\alpha$ -amylase, ligand/ $\alpha$ -glucosidase and the free ligand were -0.49 eV, -0.05 eV and -4.26 eV, respectively. Also, a passing

process has been used to investigate the charge transfer between the cavity of the receptor and the ligand. The NBO results showed a small fraction of electrons which transferred from the active site of the receptors to the ligand. These results were confirmed by the exchange of NBO charge values from +1 (protonated in the cavity of the receptors) for the free ligand to 0.94810 and 0.94344 for the ligand/ $\alpha$ -amylase and ligand/ $\alpha$ -glucosidase at the cavity of the studied active sites.

The charge density distributions of the HOMO and LUMO orbitals for the free ligand, ligand/ $\alpha$ -glucosidase and ligand/ $\alpha$ -amylase have been shown in Fig. 14. As shown in this figure, the HOMO and LUMO orbitals were distributed in the structure of the free ligand.

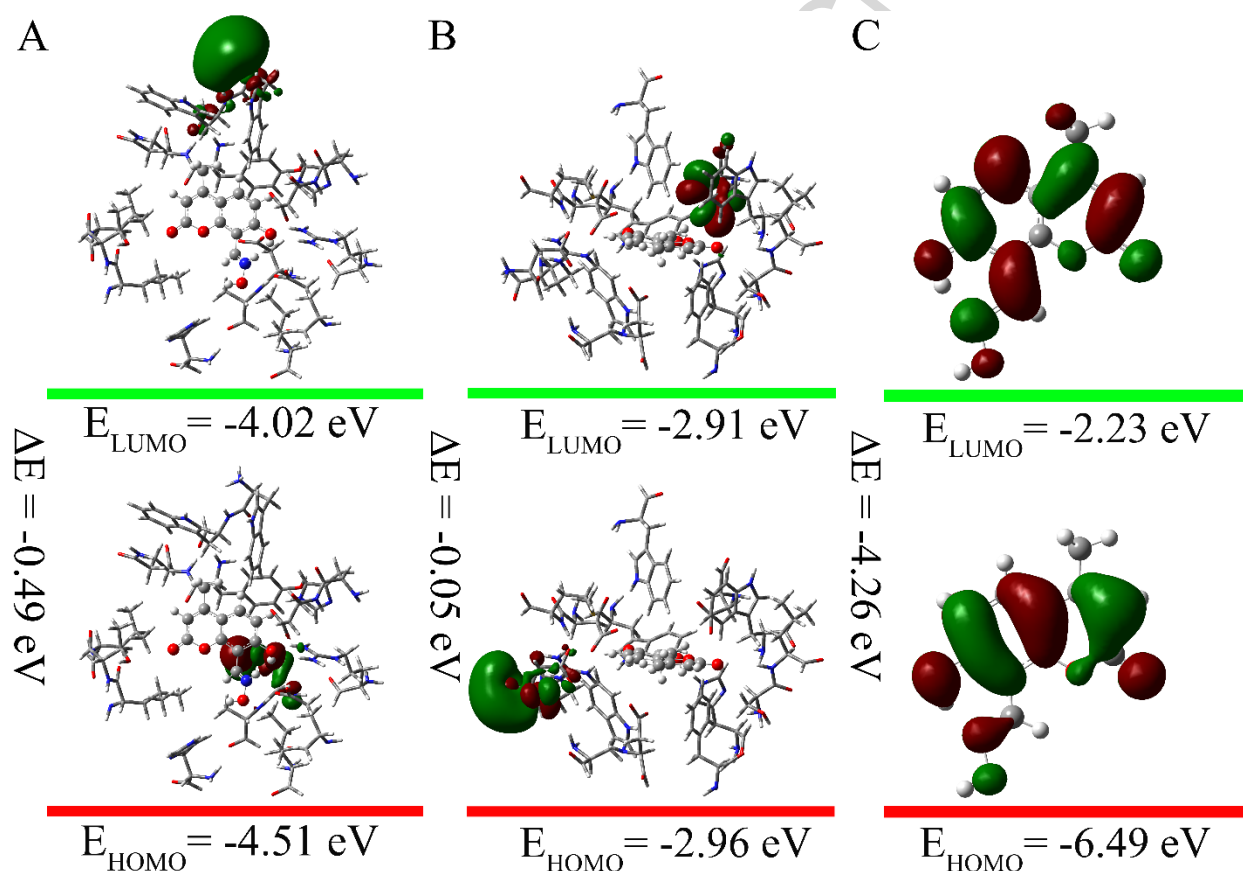


**Fig. 14.** The density distribution of the HOMO and LUMO orbitals for ligand/ $\alpha$ -amylase (A), ligand/ $\alpha$ -glucosidase (B) complexes and the free ligand (C) calculated by using B3LYP/6-311++G(d,p) level in the vacuum.

In addition, several important molecular descriptors related to the free ligand and the studied active sites; like chemical hardness ( $\eta$ ), chemical softness ( $S$ ), ionization potential ( $I$ ), the electron

affinity ( $A$ ), electronegativity ( $\chi$ ) and dipole moment (Debye); were calculated by HOMO and LUMO eigenvalues (Table 9). According to the Koopmans theorem [95, 96], these parameters were obtained from the following equations (Eqs. (8-12):

$$\eta = -\frac{(E_{HOMO} - E_{LUMO})}{2}, \text{ Eq. (8)}$$

$$S = \frac{1}{\eta}, \text{ Eq. (9)}$$

$$I = -E_{HOMO}, \text{ Eq. (10)}$$

$$A = -E_{LUMO}, \text{ Eq. (11)}$$

$$\chi = \frac{(I + A)}{2}, \text{ Eq. (12)}$$

Zhou and Parr [97] reported that the chemical hardness ( $\eta$ ) is a determining factor for the stability of a compound. This parameter is defined as the resistance of a system against charge transfer. In other word, charge transfer decreases by increasing the value of  $\eta$  [98].

**Table 9.** The HOMO-LUMO energy, chemical hardness ( $\eta$ ), chemical softness ( $S$ ), ionization potential ( $I$ ), the electron affinity ( $A$ ), electronegativity ( $\chi$ ) and dipole moment (Debye) of the free ligand and ligand/receptors ( $\alpha$ -amylase and  $\alpha$ -glucosidase) calculated by using B3LYP method with 6-311++G(d,p) basis set in the vacuum.

Parameters	Values		
	ligand	ligand/ $\alpha$ -amylase	ligand/ $\alpha$ -glucosidase
Energetic terms			
HOMO <sup>a</sup> (eV)	-6.4900	-4.5100	-2.9600
LUMO <sup>b</sup> (eV)	-2.2300	-4.0200	-2.9100
Energy HOMO-LUMO gap	-4.2600	-0.4900	-0.0500
Ionization potential ( $I$ )	6.4900	4.5100	2.9600
Electron affinity ( $A$ )	2.2300	4.0200	2.9100
Electronegativity ( $\chi$ )	4.3600	4.2650	2.9350
Chemical hardness ( $h$ )	2.1300	0.2450	0.0250
Chemical softness ( $S$ )	0.4695	4.0816	40.0000
Dipole moment (Debye)	4.3627	63.2063	106.0704

<sup>a</sup> Energy of the Highest Occupied Molecular Orbital.

<sup>b</sup> Energy of the Lowest Unoccupied Molecular Orbital.

### 3.10. Drug-likeness and ADMET prediction

To confirm the ability of 7-Oxime to act as a possible drug, the Drug-likeness of the title compound was investigated using Lipinski's rule of five [99] (Table 10). The title compound passed Lipinski's filter, and the ADMET (absorption, distribution, metabolism, excretion and toxicity) property was checked. According to this prediction, the mentioned compound doesn't have significant toxicity

and; like other coumarins; can be considered as supplementary agent to be used in therapeutic programs. However, further validation assays using *in vitro* and *in vivo* models are highly recommended to display the exact anti-diabetic potential of this compound.

**Table 10.** ADMET data and drug-likeness of 7-Oxime

A	B	C	D	E	F	G	H	I	J
219.20	-2.548	3	0	1.95	Yes	Yes	Non mutagen	-0.804	3

A: Molecular Weight, B: ADMET Solubility (aqueous), C: ADMET solubility level, D: ADMET absorption level <sup>1</sup>, E: ADMET\_A logP98, F: Lipinski's filter, G: Druglikeness, inference, H: Ames mutagenicity, I: ADMET\_BBB, J: ADMET\_BBB\_level <sup>2</sup>

<sup>1</sup> ADMET absorption level: 0: good absorption; 1: moderate absorption; 2: low absorption; 3: very low absorption [100], <sup>2</sup> ADMET\_BBB\_level: 0: Very high; 1: high; 2: Medium; 3: Low [101]

#### 4. Conclusion

In conclusion, 7- oxime was successfully prepared and characterized by <sup>1</sup>H, <sup>13</sup>C NMR, FT-IR and FT-Raman spectroscopy. Then, the vibrational bands observed in the FT-IR and FT-Raman spectrum of this compound were assigned based on the potential energy distribution (PED) and supported by calculated (scaled) DFT vibrational spectra. The comparison of the experimental and calculated spectra of the title molecule revealed that the calculated scaled results (obtained by DFT/6-311++G(d,p) method) were in good agreement with the experimental ones. In addition, comparing the NBO analysis of the monomer with those of the dimer clearly confirmed that these molecules were more stable in the dimer form and strong intermolecular hydrogen bonds existed between each two monomers. Our results also suggest that 7-Oxime was not a toxic compound and has good features to select as a lead compound in drug discovery programs. Also, molecular docking results indicated that the mentioned compound has high affinity to interact with enzymes involved in T2DM. To confirm the possible anti-diabetic activity of this compound, further animal studies are highly recommended.

#### 5. Conflict of interest

The authors declare that there is no conflict of interest regarding this publication.

#### 6. Acknowledgments

We gratefully acknowledge the financial support from the Research Council of Arak University. The instructive comments and invaluable help provided by the anonymous reviewers are also greatly appreciated

## 7. References

- [1] A.M.K. El-Dean, R.M. Zaki, A.A. Geies, S.M. Radwan, M.S. Tolba, Synthesis and antimicrobial activity of new heterocyclic compounds containing thieno [3, 2-c] coumarin and pyrazolo [4, 3-c] coumarin frameworks, *Russ J Bioorgan Chem*, 39 (2013) 553-564.
- [2] R.M. Zaki, Y.A. Elossaily, A.K. El-Dean, Synthesis and antimicrobial activity of novel benzo [f] coumarin compounds, *Russ J Bioorgan Chem.*, 38 (2012) 639-646.
- [3] A. Sánchez-Recillas, G. Navarrete-Vázquez, S. Hidalgo-Figueroa, M.Y. Rios, M. Ibarra-Barajas, S. Estrada-Soto, Semisynthesis, ex vivo evaluation, and SAR studies of coumarin derivatives as potential antiasthmatic drugs, *Eur. J. Med. Chem.*, 77 (2014) 400-408.
- [4] M.Y. Ali, S. Jannat, H.A. Jung, H.O. Jeong, H.Y. Chung, J.S. Choi, Coumarins from *Angelica decursiva* inhibit  $\alpha$ -glucosidase activity and protein tyrosine phosphatase 1B, *Chem.-Biol. Interact.*, 252 (2016) 93-101.
- [5] D. Cooke, B. Fitzpatrick, R. O’Kennedy, T. McCormack, D.i. Egan, Coumarins-Multifaceted Molecules with Many Analytical and Other Applications. , in: *Coumarins: Biology, Applications and Mode of Action*, Chichester: John Wiley & Sons, 1997, pp. 303-332.
- [6] A.C. Wallace, R.A. Laskowski, J.M. Thornton, LIGPLOT: a program to generate schematic diagrams of protein-ligand interactions, *Protein Eng*, 8 (1995) 127-134.
- [7] L. Yang, W. Ding, Y. Xu, D. Wu, S. Li, J. Chen, B. Guo, New insights into the antibacterial activity of hydroxycoumarins against *Ralstonia solanacearum*, *Molecules*, 21 (2016) 468.
- [8] A.R. Leach, *Molecular modelling: principles and applications*, Pearson education, 2001.
- [9] H. Rasouli, S.M.-B. Hosseini-Ghazvini, H. Adibi, R. Khodarahmi, Differential  $\alpha$ -amylase/ $\alpha$ -glucosidase inhibitory activities of plant-derived phenolic compounds: a virtual screening perspective for the treatment of obesity and diabetes, *Food Funct*, 8 (2017) 1942-1954.
- [10] R. Parr, W. Yang, *Density-Functional Theory of Atoms and Molecules* Oxford Univ, Press, New York, (1989).
- [11] K. Wolinski, J.F. Hinton, P. Pulay, Efficient implementation of the gauge-independent atomic orbital method for NMR chemical shift calculations, *J. Am. Chem. Soc* 112 (1990) 8251-8260.
- [12] M. Kofranek, T. Kovář, H. Lischka, A. Karpfen, Ab initio studies on heterocyclic conjugated polymers: structure and vibrational spectra of thiophene, oligothiophenes and polythiophene, *J Mol Struct.*, 259 (1992) 181-198.
- [13] H. Moghanian, A. Mobinikhaledi, R. Monjezi, Synthesis, spectroscopy (vibrational, NMR and UV–vis) studies, HOMO–LUMO and NBO analysis of 8-formyl-7-hydroxy-4-methylcoumarin by ab initio calculations, *J. Mol. Struct*, 1052 (2013) 135-145.
- [14] M.S. Manhas, S.N. Ganguly, S. Mukherjee, A.K. Jain, A.K. Bose, Microwave initiated reactions: Pechmann coumarin synthesis, Biginelli reaction, and acylation, *Tetrahedron Lett.*, 47 (2006) 2423-2425.
- [15] A. Kulkarni, S.A. Patil, P.S. Badami, Synthesis, characterization, DNA cleavage and in vitro antimicrobial studies of La (III), Th (IV) and VO (IV) complexes with Schiff bases of coumarin derivatives, *Eur. J. Med. Chem.*, 44 (2009) 2904-2912.
- [16] A.D. Becke, Becke’s three parameter hybrid method using the LYP correlation functional, *J. Chem. Phys*, 98 (1993) 5648-5652.
- [17] C. Lee, W. Yang, R.G. Parr, Development of the Colle-Salvetti correlation-energy formula into a functional of the electron density, *Phys Rev B Condens Matter*, 37 (1988) 785-789.
- [18] M. Frisch, G. Trucks, H.B. Schlegel, G. Scuseria, M. Robb, J. Cheeseman, J. Montgomery Jr, T. Vreven, K. Kudin, J. Burant, Gaussian 03, revision C. 02; Gaussian, Inc, Wallingford, CT, 26 (2004).

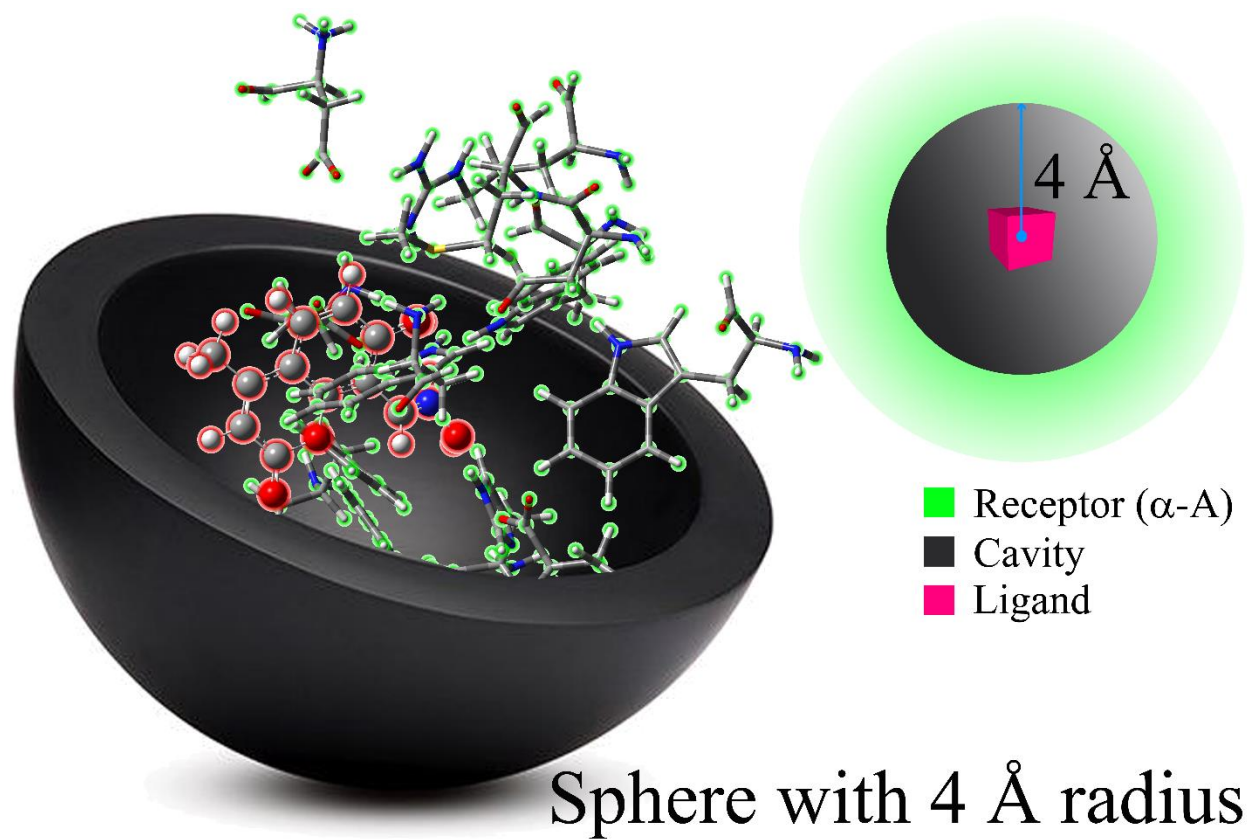
- [19] R. Dennington, T. Keith, J. Millam, GaussView, version 5, Semichem Inc., Shawnee Mission, KS, (2009).
- [20] N. Sundaraganesan, S. Ilakiamani, H. Saleem, P.M. Wojciechowski, D. Michalska, FT-Raman and FT-IR spectra, vibrational assignments and density functional studies of 5-bromo-2-nitropyridine, *Spectrochim Acta A Mol Biomol Spectrosc* 61 (2005) 2995-3001.
- [21] M.H. Jamróz, Vibrational energy distribution analysis (VEDA): scopes and limitations, *Spectrochim Acta A Mol Biomol Spectrosc* 114 (2013) 220-230.
- [22] G. Keresztury, S. Holly, G. Besenyi, J. Varga, A. Wang, J. Durig, Vibrational spectra of monothiocarbamates-II. IR and Raman spectra, vibrational assignment, conformational analysis and ab initio calculations of S-methyl-N, N-dimethylthiocarbamate, *Spectrochim Acta A Mol Spectrosc* 49 (1993) 20072019-20172026.
- [23] J.M. Chalmers, *Spectra–Structure Correlations: Polymer Spectra*, Handbook of Vibrational Spectroscopy, (2002).
- [24] E. Glendening, J. Badenhoop, A. Reed, J. Carpenter, J. Bohmann, C. Morales, F. Weinhold, NBO 5.0; Theoretical Chemistry Institute, University of Wisconsin: Madison, WI, 2001, (2004).
- [25] R. Ditchfield, Molecular orbital theory of magnetic shielding and magnetic susceptibility, *J. Chem. Phys.*, 56 (1972) 5688-5691.
- [26] H. Rasouli, S. Parvaneh, A. Mahnam, M. Rastegari-Pouyani, Z. Hoseinkhani, K. Mansouri, Anti-angiogenic potential of trypsin inhibitor purified from *Cucumis melo* seeds: Homology modeling and molecular docking perspective, *Int. J. Biol. Macromol.*, 96 (2017) 118-128.
- [27] H. Rasouli, M. Mehrabi, S.S. Arab, R. Khodarahmi, Are Pro8/Pro18 really critical for functional dynamic behavior of human endostatin N-terminal peptide? A comparative molecular dynamics study, *J. Iran. Chem. Soc.*, 14 (2017) 2023-2039.
- [28] T. Karthick, P. Tandon, K. Srivastava, S. Singh, Evaluation of non-covalent interactions of chlorambucil (monomer and dimer) and its interaction with biological targets: Vibrational frequency shift, electron density topological and automated docking analysis, *Arab J Chem*, (2017) 1-18.
- [29] T. Karthick, P. Tandon, Computational approaches to find the active binding sites of biological targets against busulfan, *J Mol Model* 22 (2016) 142-151.
- [30] H.-R. Mohammadi-Motlagh, Y. Shokohinia, M. Mojarrab, H. Rasouli, A. Mostafaie, 2-Methylpyridine-1-ium-1-sulfonate from *Allium hirtifolium*: An anti-angiogenic compound which inhibits growth of MCF-7 and MDA-MB-231 cells through cell cycle arrest and apoptosis induction, *Biomed Pharmacother* 93 (2017) 117-129.
- [31] B.K. Shoichet, S.L. McGovern, B. Wei, J.J. Irwin, Lead discovery using molecular docking, *Curr Opin Chem Biol* 6(2002) 439-446.
- [32] E. Yuriev, P.A. Ramsland, Latest developments in molecular docking: 2010–2011 in review, *J. Mol. Recognit* 26 (2013) 215-239.
- [33] V. Roig-Zamboni, B. Cobucci-Ponzano, R. Iacono, M.C. Ferrara, S. Germany, Y. Bourne, G. Parenti, M. Moracci, G. Sulzenbacher, Structure of human lysosomal acid  $\alpha$ -glucosidase—a guide for the treatment of Pompe disease, *Nat. Commun.*, 8 (2017) 1111.
- [34] G.D. Brayer, Y. Luo, S.G. Withers, The structure of human pancreatic  $\alpha$ -amylase at 1.8 Å resolution and comparisons with related enzymes, *Protein Sci*, 4 (1995) 1730-1742.
- [35] G.M. Morris, R. Huey, W. Lindstrom, M.F. Sanner, R.K. Belew, D.S. Goodsell, A.J. Olson, AutoDock4 and AutoDockTools4: Automated docking with selective receptor flexibility, *J. Comput. Chem.*, 30 (2009) 2785-2791.
- [36] G.R. Bickerton, G.V. Paolini, J. Besnard, S. Muresan, A.L. Hopkins, Quantifying the chemical beauty of drugs, *Nat. Chem*, 4 (2012) 90-98.
- [37] R. Brenk, A. Schipani, D. James, A. Krasowski, I.H. Gilbert, J. Frearson, P.G. Wyatt, Lessons learnt from assembling screening libraries for drug discovery for neglected diseases, *ChemMedChem*, 3 (2008) 435-444.

- [38] H. Yuvaraj, D. Gayathri, R.G. Kalkhambkar, G. Kulkarni, R.M. Bapset, 8-[(Hydrazinylidene) methyl]-4-methyl-2-oxo-2H-chromen-7-yl 4-methylbenzenesulfonate, *Acta Crystallogr Sect E Struct Rep Online*, 67 (2011) o323-o323.
- [39] D. Sajan, H. Ravindra, N. Misra, I.H. Joe, Intramolecular charge transfer and hydrogen bonding interactions of nonlinear optical material N-benzoyl glycine: vibrational spectral study, *Vib. Spectrosc*, 54 (2010) 72-80.
- [40] D.L. Pavia, G.M. Lampman, G.S. Kriz, J.A. Vyvyan, *Introduction to spectroscopy*, Cengage Learning, 2008.
- [41] B.H. Stuart, Organic molecules, in: *Infrared spectroscopy: Fundamentals and applications*, 2004, pp. 71-93.
- [42] P.C. Babu, N. Sundaraganesan, Ö. Dereli, E. Türkkan, FT-IR, FT-Raman spectra, density functional computations of the vibrational spectra and molecular geometry of butylated hydroxy toluene, *Spectrochim Acta A Mol Biomol Spectrosc* 79 (2011) 562-569.
- [43] S. Sebastian, S. Sylvestre, N. Sundaraganesan, M. Amalanathan, S. Ayyapan, K. Oudayakumar, B. Karthikeyan, Vibrational spectra, molecular structure, natural bond orbital, first order hyperpolarizability, TD-DFT and thermodynamic analysis of 4-amino-3-hydroxy-1-naphthalenesulfonic acid by DFT approach, *Spectrochim Acta A Mol Biomol Spectrosc* 107 (2013) 167-178.
- [44] N. Colthup, *Introduction to infrared and Raman spectroscopy*, Elsevier, 2012.
- [45] B.C. Smith, *Infrared spectral interpretation: a systematic approach*, CRC press, 1998.
- [46] G. Socrates, *Infrared and Raman characteristic group frequencies: tables and charts*, John Wiley & Sons, 2004.
- [47] M. Arivazhagana, K. Sambathkumar, S. Jeyavijayanc, Density functional theory study of FTIR and FT-Raman spectra of 7-acetoxy-4-methyl coumarin, (2010).
- [48] P. Kalsi, *Spectroscopy of organic compounds*, New Age International, 2007.
- [49] G. Varsanyi, *Vibrational spectra of benzene derivatives*, Elsevier, 1969.
- [50] N.P. Roeges, *A guide to the complete interpretation of infrared spectra of organic structures*, Wiley, 1994.
- [51] M. Govindarajan, M. Karabacak, FT-IR, FT-Raman and UV spectral investigation: Computed frequency estimation analysis and electronic structure calculations on 1-bromo-2-methylnaphthalene, *Spectrochim Acta A Mol Biomol Spectrosc* 101 (2013) 314-324.
- [52] K.M. Mukherjee, T. Misra, Surface-Enhanced Raman Spectra of 2- and 3-Hydroxypyridines in Silver Sol, *J. Raman Spectrosc* 27 (1996) 595-600.
- [53] D. Hadzi, Infrared spectra and structure of some quinone monoximes, *J. Chem. Soc.*, (1956) 2725-2731.
- [54] M. Karabacak, E. Şahin, M. Çınar, I. Erol, M. Kurt, X-ray, FT-Raman, FT-IR spectra and ab initio HF, DFT calculations of 2-[(5-methylisoxazol-3-yl) amino]-2-oxo-ethyl methacrylate, *J. Mol. Struct* 886 (2008) 148-157.
- [55] V. Krishnakumar, S. Dheivamalar, Density functional theory study of Fourier transform infrared and Raman spectra of 2-amino-5-chloro benzonitrile, *Spectrochim Acta A Mol Biomol Spectrosc* 71 (2008) 465-470.
- [56] Y. Umar, T. Jimoh, M. Morsy, Ab initio and density functional calculations of the structures and vibrational spectra of formaldoxime, *J Mol Struct Theochem*, 725 (2005) 157-161.
- [57] N. Trendafilova, G. Bauer, I. Georgieva, V. Delchev, Conformational stability and vibrational spectrum of glyoxilic acid oxime predicted from ab initio study, *J Mol Struct* 604 (2002) 211-220.
- [58] M. Albrecht, P. Zielke, C.A. Rice, M.A. Suhm, Variations of bite angle and coupling patterns in double hydrogen bonds: The case of oxime dimers, *J Mol Struct* 880 (2008) 2-13.
- [59] G. Varsányi, *Assignments for vibrational spectra of seven hundred benzene derivatives*, Halsted Press, 1974.
- [60] T. Shimanouchi, Y. Kakiuti, I. Gamo, Out-of-Plane CH Vibrations of Benzene Derivatives, *J. Chem. Phys.*, 25 (1956) 1245-1251.

- [61] J. Andzelm, C. Kölmel, A. Klamt, Incorporation of solvent effects into density functional calculations of molecular energies and geometries, *J. Chem. Phys.*, 103 (1995) 9312-9320.
- [62] V. Barone, M. Cossi, Quantum calculation of molecular energies and energy gradients in solution by a conductor solvent model, *J. Phys. Chem. A*, 102 (1998) 1995-2001.
- [63] M. Cossi, N. Rega, G. Scalmani, V. Barone, Energies, structures, and electronic properties of molecules in solution with the C-PCM solvation model, *J. Comput. Chem.*, 24 (2003) 669-681.
- [64] E. Cancès, B. Mennucci, J. Tomasi, A new integral equation formalism for the polarizable continuum model: Theoretical background and applications to isotropic and anisotropic dielectrics, *J. Chem. Phys.*, 107 (1997) 3032-3041.
- [65] X.-H. Li, X.-Z. Zhang, The spectroscopic, NMR analysis of 2-dicyanovinyl-5-(4-methoxyphenyl) thiophene by density functional method, *Spectrochim Acta A Mol Biomol Spectrosc* 105 (2013) 280-287.
- [66] H.-O. Kalinowski, S. Berger, S. Braun, Carbon-13 NMR spectroscopy, (1988).
- [67] C. James, A.A. Raj, R. Reghunathan, V. Jayakumar, I.H. Joe, Structural conformation and vibrational spectroscopic studies of 2, 6-bis (p-N, N-dimethyl benzylidene) cyclohexanone using density functional theory, *J. Raman Spectrosc*, 37 (2006) 1381-1392.
- [68] E.H. Avdović, D. Milenković, J.M. Dimitrić-Marković, N. Vuković, S.R. Trifunović, Z. Marković, Structural, spectral and NBO analysis of 3-(1-(3-hydroxypropylamino) ethylidene) chroman-2, 4-dione, *J. Mol. Struct* 1147 (2017) 69-75.
- [69] M. Szafran, A. Komasa, E. Bartoszak-Adamska, Crystal and molecular structure of 4-carboxypiperidinium chloride (4-piperidinecarboxylic acid hydrochloride), *J. Mol. Struct*, 827 (2007) 101-107.
- [70] A.E. Reed, L.A. Curtiss, F. Weinhold, Intermolecular interactions from a natural bond orbital, donor-acceptor viewpoint, *Chem. Rev.*, 88 (1988) 899-926.
- [71] N. Özdemir, B. Eren, M. Dincer, Y. Bekdemir, Experimental and ab initio computational studies on 4-(1 H-benzo [d] imidazol-2-yl)-N, N-dimethylaniline, *Mol. Phys.*, 108 (2010) 13-24.
- [72] J.B. Ott, J. Boerio-Goates, Calculations from Statistical Thermodynamics, in, Academic Press, 2000.
- [73] S.A. Kaveeshwar, J. Cornwall, The current state of diabetes mellitus in India, *Australas Med J.*, 7 (2014) 45.
- [74] F. Pociot, Type 1 diabetes genome-wide association studies: not to be lost in translation, *Clin Transl Immunology*, 6 (2017) 1-7.
- [75] A.B. Olokoba, O.A. Obateru, L.B. Olokoba, Type 2 diabetes mellitus: a review of current trends, *Oman Med J*, 27 (2012) 269-273.
- [76] M. Blair, Diabetes mellitus review, *Urol Nurs.*, 36 (2016) 27-37.
- [77] L. Bellamy, J.-P. Casas, A.D. Hingorani, D. Williams, Type 2 diabetes mellitus after gestational diabetes: a systematic review and meta-analysis, *Lancet*, 373 (2009) 1773-1779.
- [78] A.K. Tiwari, J.M. Rao, Diabetes mellitus and multiple therapeutic approaches of phytochemicals: Present status and future prospects, *Curr. Sci.*, (2002) 30-38.
- [79] M.U. Rao, M. Sreenivasulu, B. Chengaiah, K.J. Reddy, C.M. Chetty, Herbal medicines for diabetes mellitus: a review, *Int J PharmTech Res*, 2 (2010) 1883-1892.
- [80] A. Ceriello, Postprandial hyperglycemia and diabetes complications: is it time to treat?, *Diabetes*, 54 (2005) 1-7.
- [81] B. Yan, N. Raben, P. Plotz, The human acid  $\alpha$ -glucosidase gene is a novel target of the Notch-1/Hes-1 signaling pathway, *J Biol Chem*, 277 (2002) 29760-29764.
- [82] S.O. Lee, S.Z. Choi, J.H. Lee, S.H. Chung, S.H. Park, H.C. Kang, E.Y. Yang, H.J. Cho, K.R. Lee, Antidiabetic coumarin and cyclitol compounds from *Peucedanum japonicum*, *Arch Pharm Res*, 27 (2004) 1207-1210.
- [83] L. Pari, N. Rajarajeswari, Efficacy of coumarin on hepatic key enzymes of glucose metabolism in chemical induced type 2 diabetic rats, *Chem.-Biol. Interact.*, 181 (2009) 292-296.
- [84] Y. Al-Majedy, A. Al-Amiery, A.A. Kadhun, A. BakarMohamad, Antioxidant activity of coumarins, *Sys Rev Pharm*, 8 (2017) 24-30.

- [85] A. Verma, P. Dewangan, D. Kesharwani, S.P. Kela, Hypoglycemic and hypolipidemic activity of scopoletin (coumarin derivative) in streptozotocin induced diabetic rats, *Int J Pharm Sci Rev Res*, 22 (2013) 79-83.
- [86] A. Ramu, V. Vijayakumar, Antidiabetic activity of 7-methoxycoumarin from the bark of Marine plant *Rhizophora mucronata*, *Glo. Adv. Res. J. Med. Plants*, 4 (2016) 001-006.
- [87] B. Wang, N. Li, T. Liu, J. Sun, X. Wang, Synthesis and biological evaluation of novel neoflavonoid derivatives as potential antidiabetic agents, *RSC Adv.*, 7 (2017) 34448-34460.
- [88] C.H. Jhong, J. Riyaphan, S.H. Lin, Y.C. Chia, C.F. Weng, Screening alpha-glucosidase and alpha-amylase inhibitors from natural compounds by molecular docking in silico, *Biofactors*, 41 (2015) 242-251.
- [89] J.-L. Chiasson, R.G. Josse, R. Gomis, M. Hanefeld, A. Karasik, M. Laakso, S.-N.T.R. Group, Acarbose for prevention of type 2 diabetes mellitus: the STOP-NIDDM randomised trial, *Lancet*, 359 (2002) 2072-2077.
- [90] H. Ahr, M. Boberg, E. Brendel, H. Krause, W. Steinke, Pharmacokinetics of miglitol. Absorption, distribution, metabolism, and excretion following administration to rats, dogs, and man, *Arzneimittelforschung*, 47 (1997) 734-745.
- [91] R. Kawamori, N. Tajima, Y. Iwamoto, A. Kashiwagi, K. Shimamoto, K. Kaku, V.P.-S. Group, Voglibose for prevention of type 2 diabetes mellitus: a randomised, double-blind trial in Japanese individuals with impaired glucose tolerance, *Lancet*, 373 (2009) 1607-1614.
- [92] C. Rosak, G. Mertes, Critical evaluation of the role of acarbose in the treatment of diabetes: patient considerations, *Diabetes Metab Syndr Obes*, 5 (2012) 357.
- [93] H. Rasouli, M.H. Farzaei, R. Khodarahmi, Polyphenols and their benefits: A review, *Int J Food Prop*, (2017) 1-42.
- [94] H. Li, Y. Yao, L. Li, Coumarins as potential antidiabetic agents, *J. Pharm. Pharmacol.*, 69 (2017) 1-12.
- [95] R.G. Parr, R.G. Pearson, Absolute hardness: companion parameter to absolute electronegativity, *J. Am. Chem. Soc* 105 (1983) 7512-7516.
- [96] R.G. Parr, L.v. Szentpaly, S. Liu, Electrophilicity index, *J. Am. Chem. Soc* 121 (1999) 1922-1924.
- [97] Z. Zhou, R.G. Parr, Activation hardness: new index for describing the orientation of electrophilic aromatic substitution, *J. Am. Chem. Soc* 112 (1990) 5720-5724.
- [98] R.G. Pearson, Recent advances in the concept of hard and soft acids and bases, *J. Chem. Educ*, 64 (1987) 561.
- [99] C.A. Lipinski, Lead-and drug-like compounds: the rule-of-five revolution, *Drug Discov Today Technol*, 1 (2004) 337-341.
- [100] S. Mondal, S.M. Mandal, T.K. Mondal, C. Sinha, Structural characterization of new Schiff bases of sulfamethoxazole and sulfathiazole, their antibacterial activity and docking computation with DHPS protein structure, *Spectrochim Acta A Mol Biomol Spectrosc*, 150 (2015) 268-279.
- [101] A. Ahmad, A. Ahmad, H. Varshney, A. Rauf, M. Rehan, N. Subbarao, A.U. Khan, Designing and synthesis of novel antimicrobial heterocyclic analogs of fatty acids, *Eur. J. Med. Chem.*, 70 (2013) 887-900.

Graphical abstract



ACCEPTED

**Highlights**

- 7-hydroxy-4-methyl-2-oxo-2*H*-chromene-8-carbaldehyde oxime has been synthesized.
- The complete vibrational assignments and spectroscopic analyses were performed.
- The druglikeness of the title compound was investigated by following Lipinski's rule of five.
- The electronic structures of ligand/receptors were investigated with the radius of 4 Å.